Alma Mater Studiorum - Università di Bologna

SCUOLA DI SCIENZE

Dipartimento di Chimica Industriale "Toso Montanari"

Corso di Laurea Magistrale in

Chimica Industriale

Curriculum: Advanced Spectroscopy in Chemistry

Classe LM-71 - Scienze e Tecnologie per la Chimica Industriale

Catalytic reduction of organic pollutants using supported metal nanoparticles

CANDIDATE
Beatsam Kwon

SUPERVISOR
Prof. Nikolaos Dimitratos

CO-SUPERVISOR
Eleonora Monti

Academic Year 2019/2020

Index

SCOPE

Metal nanoparticle catalysts have in the last decades been extensively researched for their enhanced performance compared to their bulk counterpart. Properties of nanoparticles can be controlled by modifying their size and shape as well as adding a support and stabilizing agent. In this study, preformed colloidal gold nanoparticles supported on activated carbon were tested on the reduction of 4-nitrophenol by $NaBH_4$, a model reaction for evaluating catalytic activity of metal nanoparticles and one with high significance in the remediation of industrial wastewaters. Methods of wastewater remediation are reviewed, with case studies from literature on two major reactions, ozonation and reduction, displaying the synergistic effects observed with bimetallic and trimetallic catalysts, as well as the effects of differences in metal and support. Several methods of preparation of nanoparticles are discussed, in particular, the sol immobilization technique, which was used to prepare the supported nanoparticles in this study. Different characterization techniques used in this study to evaluate the materials and spectroscopic techniques to analyze catalytic activities of the catalyst are reviewed: ultraviolet-visible (UV-Vis) spectroscopy, dynamic light scattering (DLS) analysis, X-ray diffraction (XRD) analysis and transmission electron microscopy (TEM) imaging. Optimization of catalytic parameters was carried out through modifications in the reaction setup. The effects of the molar ratio of reactants, stirring, type and amount of stabilizing agent are explored. Another important factor of an effective catalyst is its reusability and long-term stability, which was examined with suggestions for further studies. Lastly, a biochar support was newly tested for its potential as a replacement for activated carbon.

1. Introduction

1.1 Nanomaterials in Catalysis

Catalysts are materials used to increase the rate or efficiency of a reaction by lowering the activation energy of the reaction, bringing together the reactive materials, or increasing the yield of a specific product formed over another. In more recent decades, nanomaterials have become in focus for use in catalysis. Nanoparticles are assemblies of hundreds of thousands of atoms in the range of 1-100 nm in size. The first paper published on metal nanoparticle catalysts was in 1941, where polyvinyl alcohol-capped palladium and platinum nanoparticles were synthesized using H_2 to reduce the metals.[1] The year 1987 brought another breakthrough as gold nanoparticles in the size range of less than 5 nm were found to increase their activity in the oxidation of CO by O_2.[2] Nanomaterials have been researched and applied in many other fields such as electronics, medicine, information technology, fuel cells and more. One such example that has significant implications on the environment and the economy today is catalytic converters which increase the rate of catalytic combustion by making the combustion selective to avoid toxic byproducts. Characterization methods of nanoparticles have also advanced alongside nanomaterial research. Some such modern techniques include aberration-corrected electron microscopy and X-ray absorption spectroscopy which allow for characterizing downwards of single metal atoms.[3]

Among the nanomaterials, noble metal nanoparticles, with their special electronic properties, have gained attention in the field of catalysis. In the nano size range, metal particles display differences in electrical and optical properties. For example, they undergo a change in the reduction potential based on the particle sizes due to a more negative Fermi potential, allowing them to catalyse various electron transfer reactions.[4] The high surface area and dispersion, or the ratio of the number of atoms on the surface to the total number of atoms, of metal nanoparticles also provide an

advantage over bulk metals. Metal nanoparticle catalysts display varying properties that depend on their size, shape and structure. These factors are controlled by modifications of preparation conditions. They can also be functionalized by modifying organic polymers hybridized with the metal nanoparticles. Bimetallic and multi-metallic nanoparticles can be formed as well, widening the range of compositions and structures which influence catalytic activity.

Various metal nanoparticles have been investigated for their suitability as catalysts for different reactions and conditions. Gold nanoparticles are commonly researched because they display high catalytic activity at mild conditions and ambient temperatures.[5] Amongst all metal nanoparticles, they are one of the most stable and therefore leaching of the metal to the effluent is not of concern. One major challenge of gold nanoparticles as catalysts is their tendency to aggregate. Functionalization of nanoparticles using surface-bound ligands or polymers as stabilizers improves their stability but it, in turn, leads to partial blockage of the active sites, reducing catalytic activity.[7] Therefore, the chain length and packing density of stabilizers are taken into consideration. It has been shown that high molecular weight and decreasing surface coverage of the stabilizer correlated with high rate constants as well as low induction time.[7] Nanoparticles can also be deposited onto a support and subsequently treated to remove the stabilizer, but there can be a trade-off between the stability of the nanoparticles and their catalytic activity due to the surface sites becoming deactivated.[8,9] The impact of stabilizers on the catalytic activity of these nanoparticles requires further exploration.[7]

1.2 Main preparation methods of nanoparticles

1.2.1 Impregnation

Impregnation is one of the more commonly used methods for its simplicity and low cost. This method involves wetting the support in solution with the metal nanoparticle precursor by dissolving the metal precursor in a solvent. The resulting solution with the support is in the form of a paste due to the pores of the support being filled by the metal solution. The solvent is removed by rotary evaporation and the solid is oven-dried and reduced. Using this method, however, AuNPs with a narrow particle size distribution range are difficult to obtain. Often, poorly dispersed particles with large agglomerates are seen as a result of impregnation, depending on the choice of heat treatment method (under air/O_2 or H_2).[10] Figure 1 shows a scheme of the impregnation method.

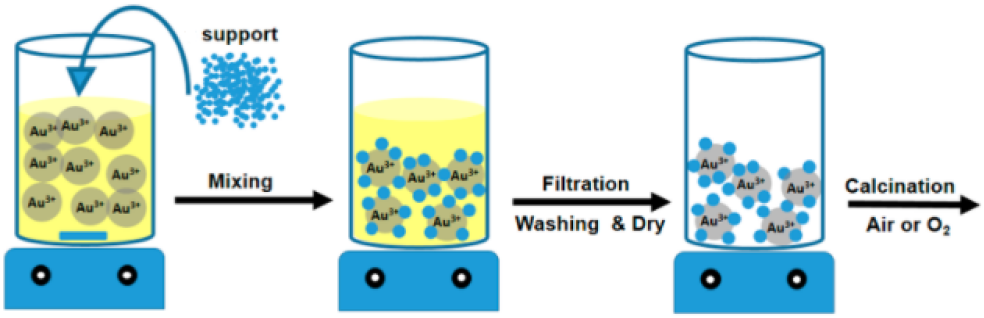

Figure 1. Scheme of impregnation method used with a metal oxide support.[11]

1.2.2 Anion adsorption

In this method, the adsorption of the metal precursor is performed at a low pH to allow its interaction with the support. When the pH of the solution is lower than the isoelectric point (IEP) or point of zero charge of the support, the overall charge of the surface of the support is positive, thus allowing for the adsorption of the anions from the metal precursor solution.[12] When the pH of the solution is higher than the IEP of the support, the overall charge is negative, allowing for the adsorption of cations. In using $HAuCl_4$ with a carbon support, the gold precursor solution is adjusted to a pH lower than that of the carbon (pH 6-8), causing the positively charged carbon

support to bind to the gold nanoparticles. Figure 2 shows changes in surface charge and the behavior of nanoparticles as a result of the change in pH.

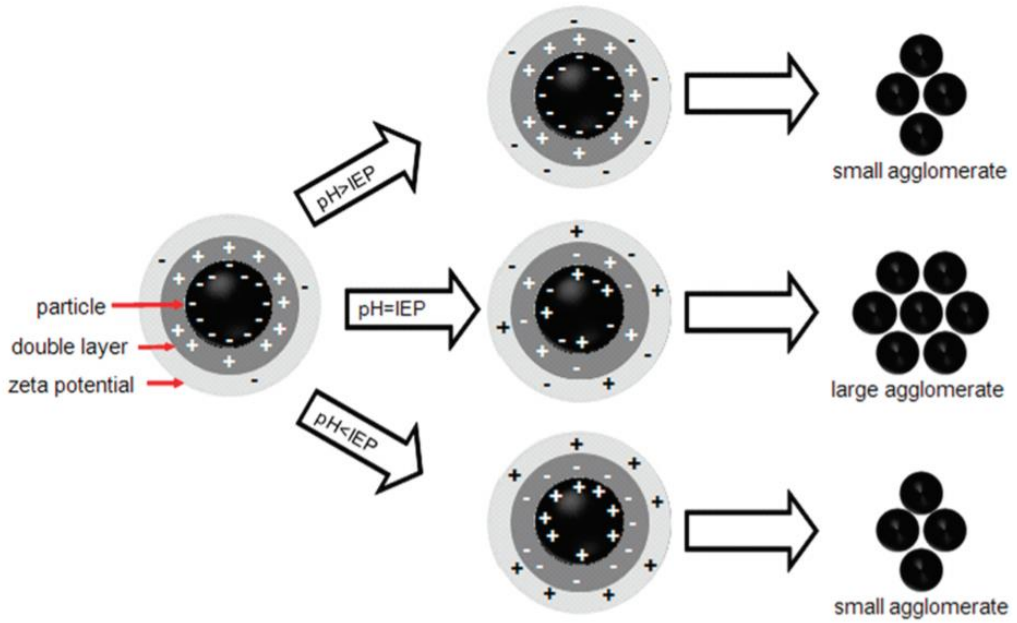

Figure 2. Scheme of the effect of pH on a metal oxide nanoparticle.[13] Surface charge and behavior of particles are altered following a change in pH.

1.2.3 Deposition precipitation

The metal precursor is dissolved in aqueous solution, the pH is adjusted to 6-10 with a base (sodium hydroxide or urea) to complete precipitation, and the precipitate is deposited on the support by adding the support under heat and constant stirring. The product is washed several times and dried in an oven before calcination. This method is not applicable to acidic and hydrophobic supports like AC due to the required pH adjustment.[14] Figure 3 shows a scheme of the deposition precipitation method.

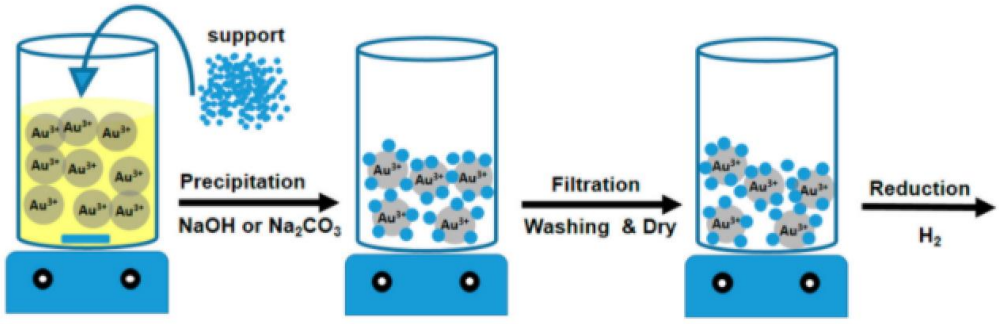

Figure 3. Scheme of the deposition precipitation method used with a metal oxide support.[11]

1.2.4 Sol immobilization

Using the methods mentioned above, the issue of metal dispersion is often encountered depending on the type of support. Sol immobilization involves the immobilization of pre-formed metallic sol, which allows for a better control of the particle size with less influence of the type of support.[15] In sol immobilization, the metal precursor is reduced, and nanoparticles are stabilized by a stabilizing agent, usually a polymer, which prevents agglomeration of the nanoparticles. Polyvinyl alcohol has been shown in several studies including ours to yield good dispersion of the nanoparticles.[15] The support is added to the metal colloidal solution to immobilize the nanoparticles. This technique overall provides the narrowest particle size distribution of the nanoparticles which is crucial for high, consistent catalytic activity. The synthesis of AuNP catalysts used in this study has been prepared using this method.

1.3 Wastewater remediation and nitrophenols

Nitrophenols are among the most common environmental pollutants with high toxicity and carcinogenic properties.[16] Among industrial plants, they are most present in wastewaters from plants producing pesticides, explosives, dyestuffs and leather treatment products. 4-nitrophenol, which is released into industrial wastewaters from agriculture and manufacturing, exhibits high

stability and solubility in wastewaters.[17] 4-nitrophenol has been reported as carcinogenic, teratogenic, and mutagenic.[18] It is one of the top 114 organic pollutants according to the United States Environmental Protection Agency.[9] The presence of the nitro group in the aromatic ring enhances its stability to degradation. 4-nitrophenol has received much attention in academic research due to its reduction to 4-aminophenol.[19] This reduction process by BH_4^- is considered a model reaction because its kinetics can be traced by UV-Vis spectroscopy and it yields one product. It is also ideal for testing the catalytic efficiency of metal nanoparticles because of its slow rate in the absence of a suitable catalyst.[18] Considering the environmental impact of 4-nitrophenol in wastewaters, the development of a highly efficient catalyst is an immensely valuable task in industrial chemistry.

With regards to nitrophenols in wastewaters, the conventional remediation approaches can be classified as physiochemical and biological, some of which include adsorption, solvent extraction, oxidation or reduction, and bioremediation with microbes. Physiochemical methods such as adsorption and solvent extraction simply concentrate the pollutants in a different phase, thus requiring subsequent treatment of the pollutants. Bioremediation, a low cost, environmentally friendly method which uses microbes to catalyze the degradation of organics, performs poorly at high concentrations of toxic organics, and the rate of degradation is slow. Moreover, the presence of heavy metals which are common in wastewater streams inhibits microbial activity.[20]

1.4 Advanced oxidation processes

Advanced oxidation processes (AOPs) use highly reactive hydroxyl radicals which non-selectively can oxidize a variety of organic pollutants into CO_2 and H_2O.[6] These radicals are highly reactive with a short lifetime, meaning they increase reaction rates and do not accumulate in the medium.[21]

AOPs are often combined with ozone, catalysts, UV radiation, microwave or ultrasound for a faster and more efficient treatment and are often capable of complete mineralization of organics. Therefore, AOPs are an attractive solution to compounds with high stability, toxicity and non-biodegradability.

Among AOPs, the Fenton process is known to be one of the most effective in terms of the wide variety of organics that can be treated as well as the short reaction time.[22] In the Fenton process, Fe^{2+} is oxidized to Fe^{3+} by hydrogen peroxide, providing hydroxyl radicals and hydroxides which accelerate the oxidation process. The degree of mineralization, however, is not optimal and can vary considerably based on the amount of reagent used and the presence of UV radiation (Photo-Fenton). A simple schematic of the Fenton process is shown in Figure 4.

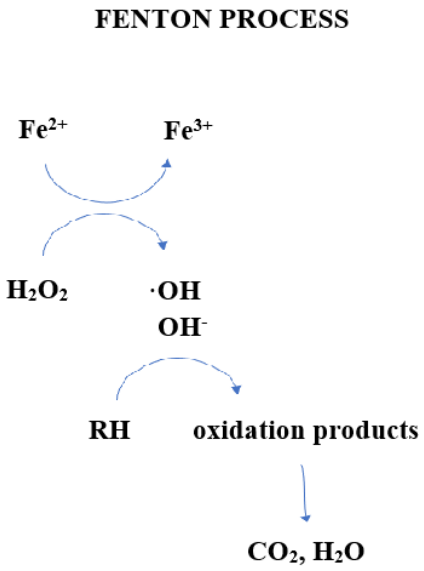

Figure 4. Reaction scheme of the Fenton oxidation process.

Processes that use UV and a catalyst, photocatalytic decomposition, involve photoexcitation which generates positively charged electron holes in the catalyst, which interact on the surface with H_2O or hydroxides to produce hydroxyl radicals. Photocatalysis has been improved by using

semiconductor materials. Specifically, TiO_2 photocatalysts are the most effective in treating nitrophenols in waters due to low toxicity, high stability, ease of availability and superior performance.[23] TiO_2-based photocatalysis produces more hydroxyl radicals compared to other AOPs.[23]

Although AOP technology has advanced with the research of different catalysts and is regarded as a powerful method of wastewater treatment, the application of AOPs at an industrial scale can be impractical cost wise. The expenses of catalyst and energy consumption in the generation of ozone or UV radiation are practical for a more selective treatment of specific targets. Another challenge to consider is the high reactivity and low selectivity of radicals used in AOPs. Due to the high natural organic content of wastewaters and the low concentrations of toxic organic pollutants, AOPs may not be the ideal method of wastewater remediation because organic matter is non-selectively oxidized.

1.5 Ozonation of 4-nitrophenol using metal nanoparticles

AOPs at the laboratory scale have shown to be highly efficient in treating organic compounds present in low levels in wastewaters. Various advanced oxidation processes (AOPs) for the treatment of organics such as ultrasonic, photooxidation, Fenton, and wet oxidation exist. However, many of these processes are limited in applications in the industrial scale due to economic and technical considerations. Among these AOPs used to generate strong oxidants for degradation of organics, ozonation is commonly used to treat toxic compounds in wastewaters. Ozonation processes involve partial or, in some cases, complete oxidation of organic compounds. Oxidation using hydroxyl radicals occurs rapidly owing to their high oxidizing potential, whereas ozonation has a smaller potential. However, with high dosages and long reaction times, ozone can

oxidize some organic compounds to CO_2 and H_2O with some inorganic salts. Although most ozonation reactions oxidize one organic compound to another, the resulting shorter and simpler organic products makes them more biodegradable.[24]

Although ozonation is one of the most widely used processes, it is not without limitations. In some cases, toxic intermediates result from ozonation processes and a careful control is needed in the utilization of ozone in the laboratory. In response to this, catalytic ozonation has emerged as a more suitable method of organic compound degradation. Phenols, with their electron-donating -OH group, are highly reactive to ozone with the carbon in the ortho- and para- positions. When 4-nitrophenol undergoes electrophilic attack by ozone or hydroxyl radicals, it forms quinone intermediates, which later break down into smaller compounds such as maleic acid, oxalic acid, acetic acid and formic acid, eventually yielding CO_2 and water. However, oxalic acid does not further breakdown with exposure to ozone without the presence of a catalyst. Catalytic ozonation can avoid the build-up of oxalic acid in wastewaters. It also offsets the limitations of the costs of high energy consumption and low efficiency due to the reaction kinetics of ozonation.[25] Gu et al. proposed a reaction pathway of 4-nitrophenol degradation by ozone-based AOP, organized in Figure 5. The applied catalyst increases the decomposition of soluble ozone to produce highly reactive hydroxyl radicals.[26]

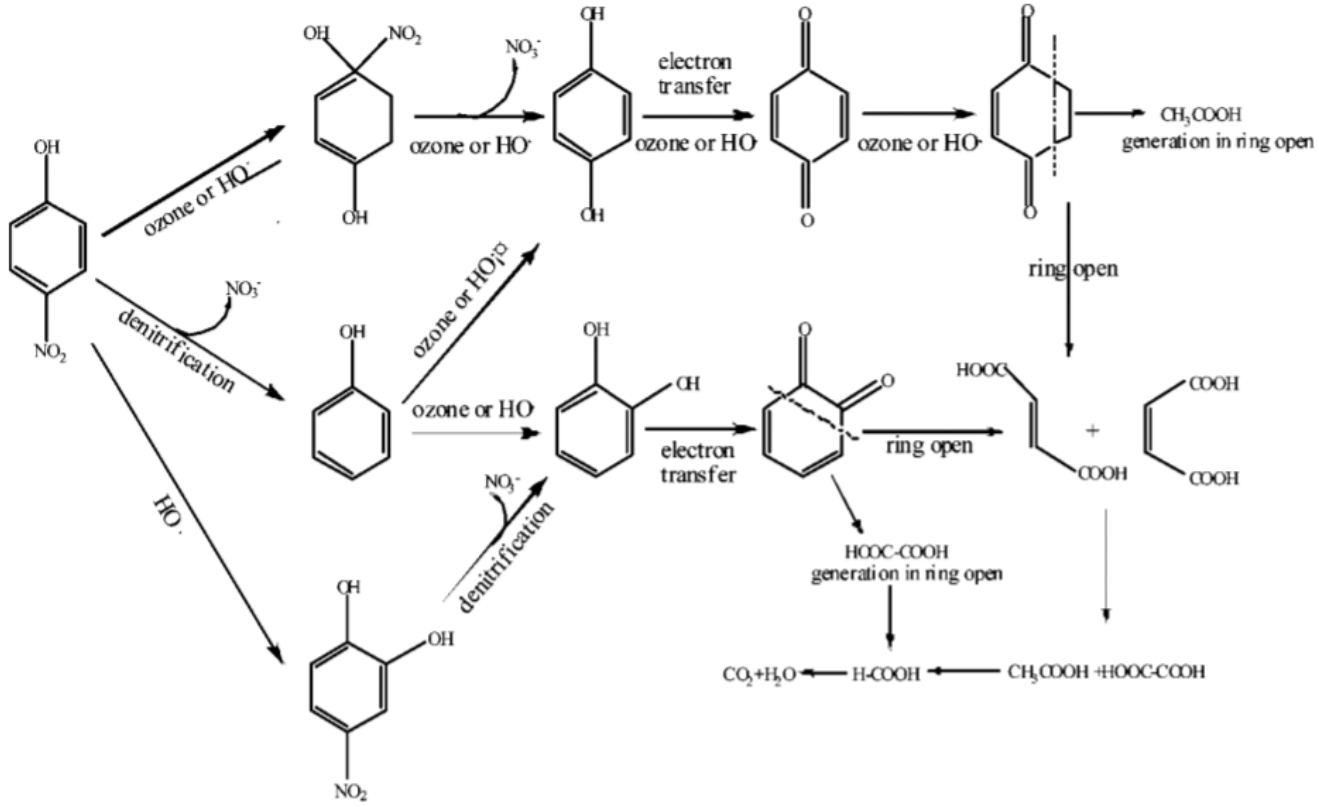

Figure 5. Proposed 4-nitrophenol degradation by ozone-based AOPs by Gu et al.[72]

1.5.1 Heterogeneous Catalytic Ozonation

Ozone exhibits low solubility and stability in water. It is also selective in its oxidative process. With the addition of a catalyst, ozone reacts with water to generate hydroxyl radicals, thus increasing the reaction rate. Heterogeneous catalytic ozonation offers more benefits than homogeneous due to the catalyst recycling potential and/or the ease of separation after a reaction. As opposed to homogeneous catalytic ozonation, in which ozone is activated by aqueous metal ions in the presence of UV radiation, heterogeneous catalytic ozonation occurs in the absence of UV. Metals and metal oxides are the most used catalysts in the heterogeneous catalytic ozonation process.

Although there have been many studies reported using homogeneous catalysts such as Mn^{2+}, Fe^{3+}, Fe^{2+}, Cd^{2+}, Cu^{2+}, Zn^{2+}, Cr^{2+}, Co^{2+} and Ag^{+}, one major limitation of homogeneous catalysts in these processes is the high consumption of catalyst.[27,28] Heterogeneous catalysts have shown to not only be more easily recycled for further use, but also to increase the efficiency of the reaction by the adsorptive and oxidative properties of solid metals. They have proven effective in wastewater treatment plant applications.[29]

The reaction is carried out in a stainless steel or glass reactor at room temperature and ambient pH which is adjusted as needed. The ozone generator, with an adjustable gas flow rate, is connected to the reactor. The ozone monitor detects the dissolved ozone concentration. Samples are collected at regular time intervals and treated with nitrogen gas to remove residual ozone. The sample is filtered and analyzed on the UV-Vis. A schematic of ozone flow from the oxygen supply to ozone quenching post-reaction is shown in Figure 6.

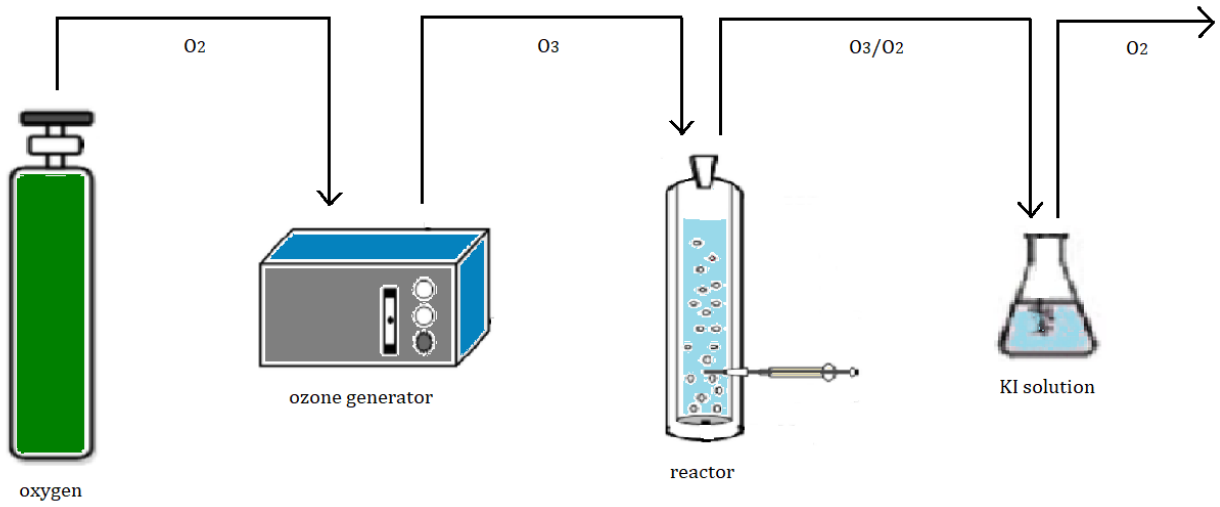

Figure 6. Setup of ozonation reaction.

1.5.2 Catalytic approaches (Case studies)

Ozonation reactions from literature using monometallic vs. bimetallic catalysts are reviewed and compared with simple ozonation (Table 1).

TiO_2-Fe_3O_4

One approach to overcome the drawback of recovering solid catalysts from aqueous phase is to introduce a magnetic component in the catalyst. A magnetically separable TiO_2-Fe_3O_4 composite was synthesized.[30]

- **Synthesis of catalyst**

  To synthesize the composite catalyst, titania was added to an isopropyl alcohol solution of suspended magnetite particles and mixed at 60℃. After mixing and cooling, distilled water was added to hydrolyze the titania, followed by more mixing at 60℃. The precipitate was filtered, rinsed with isopropyl alcohol and dried.

- **Characterization**

  Surface area and pore volume of catalyst samples by BET method (457 m^2/g; 0.74 cm^3/g) were determined. Average particle sizes were measured using XRD and SEM (144 nm), and FTIR spectra were recorded.

- **Oxidation reaction**

  In a glass cylindrical reactor, 10 mg/L of ozone was supplied at a flow rate of 0.8 L/min. Aqueous 4-nitrophenol solution was 400 mg/L, and the catalyst added was 1.2 g/L.

- **Reusability**

  Magnetic separation of the composite was achieved by exposing the aqueous suspension to a magnetic field for 3 min. The recovered catalyst was reused in further reactions, losing approximately 4% activity per cycle on average.

- **Results**

Increase in magnetite content over 30% wt. resulted in a decrease in catalyst activity, likely due to increased magnetite on the surface of the composite, hindering the reaction. Within 70 min, approximately 50% of 4-nitrophenol was degraded. Within 180 min, complete degradation was achieved. The composite catalytic activity outperformed those of the monometallic and simple ozonation without any catalyst.

ZnO

Ozonation of 4-nitrophenol without a catalyst and ozonation combined with nano-ZnO were compared.[31] In accordance with previous studies, it was found that the metal catalyst improved the efficiency of the ozonation reaction by initiating the decomposition of ozone.[32]

- **Synthesis of catalyst**

  Nano-ZnO (<100 nm) was used as is.

- **Characterization**

  No characterization method is mentioned.

- **Oxidation reaction**

  In a semi-batch stirred reactor, ozone was continuously supplied into a 2000 ml glass reactor. The 1000 ml reaction solution contained 16 mg of 4-nitrophenol and 300 mg of ZnO diluted with deionized water and stirred with a magnetic stir bar. The ZnO was added into the solution immediately following the release of ozone into the 4-nitrophenol solution. Ozone gas flow was kept at 1000 ml/min with the ozone concentration of 5.64 mg/L. Residual 4-nitrophenol was measured using HPLC with a UV detector. The solutions were centrifuged and filtered using 0.2 μm microfilters prior to measurement.

- **Reusability**

  No reusability test was performed.

- **Results**

  The simple ozonation reaction, tested at pH 3, 7 and 9, showed increased efficiency with rising pH. At pH 9, conversion was at 76% in the first 5 minutes. The catalytic ozonation reaction with ZnO, tested at pH 3, 7 and 9, showed increased efficiency with decreasing pH. At ambient pH, conversion was at 93% in the first 5 minutes. In basic conditions, the production of OH^- ions which initiate the radical chain reaction led to the efficient degradation of 4-nitrophenol by ozone. In the catalytic ozonation, acidic conditions prevented the formation of clusters of the ZnO particles, which led to the efficient degradation of 4-nitrophenol.

TiO_2

Ozonation of 4-nitrophenol using a TiO_2 catalyst and simple ozonation were compared.[33] Effect of pH was tested, and the reaction process was analyzed using HPLC.

- **Synthesis of catalyst**

  TiO_2 (20 nm) was used as is.

- **Characterization**

  Titanium dioxide of BET surface area 55 m^2/g and average particle size 20 nm was purchased. TEM and SEM were performed to confirm average particle size.

- **Oxidation reaction**

  In a semi-batch reactor, 1000 ml of aqueous solution with 40 mg/L of 4-nitrophenol and 1 g of TiO_2 were mixed. Flow rate of ozone supply was kept constant at 0.5 L/min with an

ozone concentration of 20.8 mg/L. The reaction mixture was sampled at intervals and filtered to analyze via HPLC.

- **Reusability**

  TiO_2 particles were filtered out of the solution, washed with distilled water, dried and heated at 150℃ for two hours to remove any adsorbed molecules from the surface. Within three runs, degradation decreased from 94 to 83 and 69%.

- **Results**

  Efficient formation of hydroxyl radicals at high pH enhanced the degradation of 4-nitrophenol. At pH 9, 89.3% of 4-nitrophenol was removed within 60 min. In the catalytic ozonation, a slightly acidic pH of 5 yielded 97% degradation within 60 min. A kinetic analysis yielded a first-order rate constant of $k = 54.8*10^{-3}$ min^{-1}.

Table 1. Review of 4-nitrophenol catalytic ozonation studies.

Metals	Avg. particle size (nm)	Reusability	Simple O_3 activity	Catalyst/O_3 activity	Notes	Ref.
TiO_2-Fe_3O_4	144	Loss of 4% per cycle	Approx. 40% of TiO_2/O_3	100% in 180 min	• With Fe_3O_4, activity increased; recovery from aq. phase in 3 min • TiO_2 monometallic yielded approx. 70% of TiO_2/O_3	(30)
ZnO	<100	-	76% in 5 min	93% in 5 min	-	(31)
TiO_2	20	69% after three reuses	89% in 60 min	97% in 60 min	-	(33)

1.6 Chemical reduction of nitrophenol using metal nanoparticles

The catalytic reduction of 4-nitrophenol to 4-aminophenol has been shown to be one of the most efficient methods, owing to the fact that 4-aminophenol, the only product of the reaction, can be recycled for various purposes such as drug and dye synthesis. Paracetamol and phenacetin are some important drugs that require 4-aminophenol as an intermediate. 4-aminophenol is also used as a photographic developer and for anticorrosion purposes.[34]

The chemical reduction of 4-nitrophenol by $NaBH_4$ does not proceed in the absence of a catalyst due to the kinetic barrier between the repelling negative ions of 4-nitrophenol and borohydride. This makes the reduction reaction an accurate gauge for evaluating the performance of the catalyst. It follows the Langmuir-Hinshelwood model, which was first proposed by Wunder et al. to provide the mechanism for metal nanoparticle catalytic reduction of 4-nitrophenol by $NaBH_4$.[35] According to this model, the catalytic reduction occurs on the surface of metallic nanoparticles. The BH_4^- ions and 4-nitrophenol adsorb onto the surface, where hydrogen is transferred to the metal surface. The N-O bond of 4-nitrophenol is weakened as electrons are delocalized from the oxygen to the surface, and 4-nitrophenol is reduced to 4-aminophenol, yielding H_2O.

Au, Ag, Pt and Pd are commonly used metal nanoparticle catalysts in the reduction of organics. These noble metals are also the most used in bimetallic or multimetallic combinations. Each metal has its strengths applied as catalysts. While all of them are preferred for their stability in various reactions, AuNPs can perform in mild conditions and show a direct correlation between particle size and catalytic activity. AgNPs are desired for their high activity considering the low cost.[36] Pt and PdNPs exhibit excellent activities due to their large surface areas despite the high cost.[37] These metals in combination have attracted interest due to an enhanced catalytic performance as a result of synergistic effects and an offset of specific limitations faced with monometallic catalysts. For example, gold nanoparticles are limited in high-temperature reaction

applications due to particle aggregation upon exposure to heat.[38] Combining gold with platinum group metals such as platinum or palladium, their robustness at high temperatures and the geometry of the bimetal catalyst can limit the aggregation of gold nanoparticles. Synergistic effects of metals may be geometric, as in the example of aggregation of gold, or electronic. Because gold is the most electronegative of the transition metals, electron transfer from another metal to gold may improve its catalytic activity.[39]

1.6.1 Catalytic approaches (Case studies)

Reduction reactions from literature using mono-, bi-, multi-metallic catalysts with and without support are reviewed and compared (Table 8).

Palladium/Graphene

Chemical and mechanical properties of a catalyst can be improved with a proper support. Commonly used supports include silica, alumina, zeolites, TiO_2, polymers and carbon materials.[9] Graphene, which exhibits high surface area, electronic transport properties as well as mechanical stiffness, makes an efficient support for catalysts. Pd-based catalysts have been successfully used to hydrogenate nitrophenols.[9] The $\pi - \pi*$ stacking interactions facilitated the binding between nitrophenol derivatives and the graphene oxide, resulting in enhanced adsorption.

- **Synthesis of catalyst**

  Graphite oxide and graphene sheets were synthesized according to the Hummers method.[40] Pd/G nanocomposites with various amounts of Pd were prepared according to a hydrothermal method.[9]

- **Characterization**

  TEM images and XRD analyses determined the average particle (crystallite) size of Pd particles supported on graphene as 5.8 nm.

- **Reduction reaction**

  The reaction was conducted at room temperature. Solutions of 4-nitrophenol (0.3 mM) and $NaBH_4$ (0.1 M) were freshly prepared. 4 mg of Pd/G was added to a 40 ml 4-nitrophenol solution under ultrasound irradiation for several minutes. 3 ml of $NaBH_4$ solution was added to the mixture under stirring. 3 ml aliquots were sampled at certain time intervals and analyzed by UV-Vis spectroscopy.

- **Reusability**

  The catalyst was recovered by filtration and reused five times. The conversion rate was 85% after five reuses.

- **Results**

  Activity of catalyst decreased with increasing Pd content. Ortho-, meta- and para-substitutions of nitrophenols were used in the hydrogenation reaction, with methyl alcohol as solvent. For the *o*-NP and *p*-NP, the negative charge which is delocalized to the nitro group makes them stable and less reactive. Of the two, the *o*-NP exhibits higher reactivity due to a stronger inductive effect. 2,4-dinitrophenol and 2,4,6-trinitrophenol were also reacted. The multi-substituted nitrophenols exhibited low reactivities due to large steric hindrance. Activities are compared in Table 2.

Table 2. Activities of Pd/G catalysts with varying Pd content on *p*-NP conversion and of Pd0.05/G on various substituted NP conversion.

Catalyst	Raw material	k (min^{-1})	Catalyst	Raw material	k (min^{-1})
Pd0.05/G	*p*-NP	2.192	Pd0.05/G	*o*-NP	2.279
Pd0.10/G	*p*-NP	1.176	Pd0.05/G	*m*-NP	3.562
Pd0.20/G	*p*-NP	0.144	Pd0.05/G	*p*-NP	2.192
Pd0.05/C	*p*-NP	0.932	Pd0.05/G	2,4-DNP	0.974
			Pd0.05/G	2,4,6-TNP	0.531

AuPd/Graphene

Synthesis of Catalyst

- Graphene nanosheets were prepared according to a modified Hummer's method.[42] To synthesize AuPdNP/G, 5 ml of a G colloid (0.025 wt%) and 0.5 ml of a $HAuCl_4$ (10 mM) aqueous solution were stirred for 1 min, then 0.5 ml of K_2PdCl_4 (10 mM) aqueous solution was added to stir for 4 min at room temperature.[41] The mixture was washed with water and centrifuged to draw out the liquid phase. For comparison, different ratios of Au:Pd were also tested as well as monometallic PdNP/G and AuNP/G.

Characterization

- TEM images and XRD analyses determined the average particle size of AuPdNPs supported on graphene nanosheets as 3.46 nm (Figure 7). For the monometallic NPs, AuNPs and PdNPs had an average size of 3.15 and 2.67 nm, respectively.

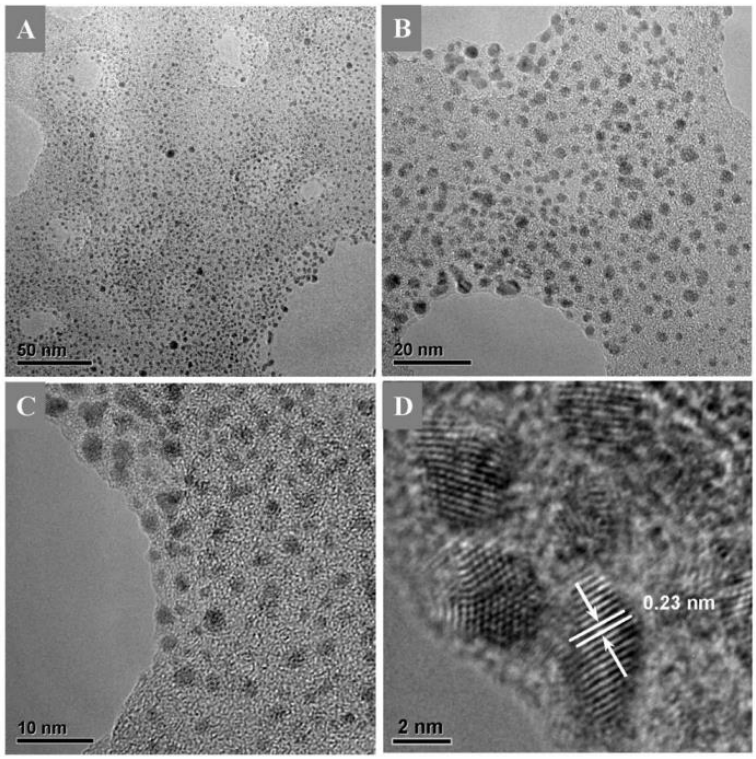

Figure 7. TEM (A-C) and HRTEM (D) images of AuPdNP/Gs.The HRTEM image shows the lattice fringe distance of 0.23 nm between the lattice spacings of Au and Pd NPs.

Reduction reaction

- 1 ml of 4-nitrophenol solution (0.1 mM) and 1.0 ml of $NaBH_4$ solution (10 mM) were mixed. 5 µl of 0.25 mg/ml AuPdNP/G (1.25 ug for 25.2 wt% Au) was added to the mixture for analysis.

Reusability

- The catalyst was reused five times without filtering. 5 ul of 20 mM 4-nitrophenol and 10 ul of 1 M $NaBH_4$ solutions were added directly to the post-reaction mixture. By the fourth run, the rate constant was approximately 91% of the first run.

Results

- PdNP/G had a faster rate of reaction than AuNP/G, but both were slower than the bimetallic AuPdNP/G. Bimetallic composites exhibited high catalytic activity, with the 1:1 Au:Pd composite having the highest (Table 3).

Table 3. *k* values of Au/G, Pd/G and AuPd/G with varying AuPd content.

	Au (wt %)	Pd (wt %)	k (min^{-1})
AuNP/G	25.7	-	0.109
Au82Pd18NP/G	22.3	2.6	0.190
Au71Pd29NP/G	24.0	5.3	0.313
Au53Pd47NP/G	25.2	12.1	0.867
Au42Pd58NP/G	23.6	17.5	0.385
Au35Pd65NP/G	25.5	25.4	0.244
PdNP/G	-	16.0	0.164

Ag/CA and Au/CA (Calcium Alginate)

Alginic acid is a biopolymer originating from brown algae. Alginate gels as a stabilizer of metal nanoparticles are affordable and possess mild reducing ability and biodegradability.[43] Its potential in green catalysis is being researched with several different metal nanoparticle catalysts.

Synthesis of Catalyst

- Ag embedded CA and Au embedded CA beads were prepared separately using a photochemical approach.[43] For Ag/CA, 3.7 g of CA gel beads were incubated with 1 ml of 1.0 mM $AgNO_3$ solution for 3 hours and irradiated with UV radiation at 365 nm for 4 terms of 10 minutes of irradiation followed by 10 minutes of gap. Beads were washed and dried for 24 hours in air with no light. For Au/CA, 1.0 mM $HAuCl_4$ was used.

Characterization

- XRD patterns confirmed the formation of single crystalline nanoparticles with no metal oxide. SEM and TEM images showed the particle morphologies and particle size. The

spherical nanoparticles had an average particle size of 7 nm for Ag, and 5 nm for Au. The possibility of alginate reacting with borohydride was investigated by performing an FTIR analysis on the catalyst after reaction and comparing it to CA spectra. No new peaks were detected.

Reduction Reaction

- 2.5 ml of 0.1 M $NaBH_4$ solution and 25 ul of $1*10^{-2}$ M 4-nitrophenol solution were mixed in a quartz cuvette, then the catalyst was added.

Reusability

- After completion of a cycle, fresh 4-nitrophenol and $NaBH_4$ solutions were added to the mixture. It was observed that up to the third cycle the catalyst efficiency increased with less time for reaction completion. After the third cycle, the efficiency remained near constant.

Results

- Ag/CA converted 99% of 4-nitrophenol within 8 minutes of reaction, and Au/CA converted 92% within 50 minutes. Rate constants for Ag/CA were $1.03\text{-}1.04*10^{-5}$ and for Au/CA $0.14\text{-}0.20*10^{-5}$.

Pt/PVPh (polyvinylphenol)

In this study, the polyvinylphenol (PVPh) molecule was used as a stabilizer for the metallic Pt nanoparticles.[44]

Synthesis of catalyst

- 1.2 ml of alkaline PVPh solution (0.8 wt%) and 5.78 ml of water were mixed at room temperature, then 1.04 ml of 10 mM H_2PtCl_6 added. The pH was maintained at 11 for one

week of magnetic stirring at room temperature. PtNPs with no PVPh were also prepared for comparison purposes by stirring 4 ml of aqueous H_2PtCl_6 solution (5 mM) at room temperature with 8 mg of $NaBH_4$ for 10 minutes. The mixture was centrifuged at 8000 rpm, and the resulting solid was vacuum dried at 70°C for 24 hours.

Characterization

- TEM images showed a narrow particle size distribution and formation of ultra-small nanoparticles of 1.6 ± 0.2 nm for the PVP-capped, and 3.5 nm for the bare Pt nanoparticles. The hydrodynamic diameter of PtNPs in solution from DLS analysis was 11.7 nm. TGA analysis was also done to see the metal loading by analyzing the weight loss of the sample in the temperature range of 120 to 700°C. Because metal NPs are thermally stable within this range, the weight loss are assumed to be entirely due to PVPh. The presence of 38.2% metallic Pt was observed.

Reduction reaction

- An aqueous suspension of Pt/PVPh of 0.1 mg catalyst in 0.8 ml of water was added to 0.1 ml of 4-nitrophenol solution (3 mM) into a 3 ml quartz cuvette under stirring at 500 rpm. To this mixture, 0.1 ml of $NaBH_4$ solution (300 mM) was added to start the reaction.

Reusability

- After each cycle, the pH was decreased to 5, the catalyst was centrifuged out and washed with water at pH 5, then re-dispersed in aqueous solution of pH 8 for reuse. There was an abrupt decrease of activity upon reuse, likely due to aggregation of the particles, as confirmed from the TEM images. By the fourth cycle, the activity was 27% of the initial.

Results

- Activities of nanoparticle catalysts with and without PVPh are compared in Table 4.

Table 4. K_{app} and k_{nor} values of catalysts synthesized with and without PVPh.

	Amount (mmol)	k_{app} (s^{-1})	k_{nor} (s^{-1} $mmol^{-1}$)
PVPh-Pt_5	$2.0* 10^{-3}$	$1.12* 10^{-2}$	5.62
Bare-Pt	$5.7* 10^{-4}$	$1.51* 10^{-3}$	2.65

Citrate-capped AgAu

The AgAu bimetallic system, among many bimetallic combinations, is of particular interest due to their stability, excellent catalytic activity, facility of synthesis, and similar crystal structures that allow the oriented formation of one metal shell over the core of another.[46]

Synthesis of catalyst

- AuNPs were prepared using the citrate thermal reduction method.[45] 1 ml of 1 wt. % aqueous solution of $HAuCl_4*3H_2O$ added to 90 ml distilled water was stirred and heated to boiling. 2 ml of sodium citrate was added as a reducing and stabilizing agent. The resulting solution was left in an ice bath and washed three times.

  The AgAuNPs were prepared using the seed colloidal method. The citrate-capped AuNPs and 1 ml of sodium citrate solution were added to 30 ml distilled water and stirred. 1.2 ml of 10 mM silver nitrate solution and 0.4 ml of 100 mM ascorbic solution were added dropwise with stirring. The solution was stirred for 30 min and washed three times.

Characterization

- TEM images showed average diameters of 24.1 ± 2.7 nm for AuNPs, 75.2 ± 5.3 nm for the bimetallic with 2.0 ml of Au seed, and 55.2 ± 6.0 nm for 5.0 ml of Au seed (Figure 8).

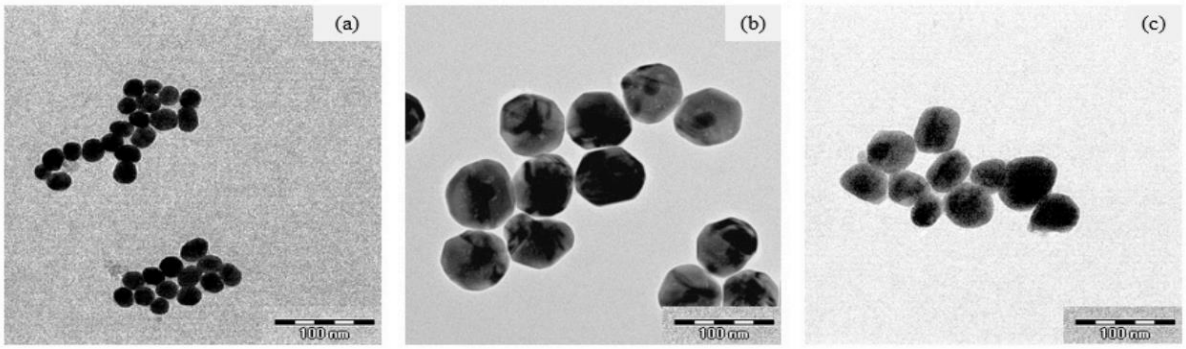

Figure 8. TEM images of AuNPs (a), AuAgNPs with 2.0 ml Au seeds (b), and AuAgNPs with 5.0 ml Au seeds (c).

Energy Dispersive X-ray Spectroscopy (EDS) analysis confirmed the presence of Ag and Au in the nanoparticles.

High-Angle Annular Dark-Field Scanning Transmission Electron Microscopy (HAADF-STEM) images showed a stark contrast between the brightly shown heavier Au and the lighter Ag.

Reduction reaction

- The reaction was carried out in a quartz cuvette with 3.0 ml of 0.2 mM 4-nitrophenol, 1.0 ml distilled water, and 0.5 ml of 0.4 M $NaBH_4$ solution. 0.2 ml of the catalyst was added to initiate the reaction.

Reusability

- Reusability test was not performed.

Results

- Activities of AuNPs and AgAuNPs with differing amounts of Au are compared in Table 5.

Table 5. K_{app}, reaction times and particle sizes of nanoparticles.

	K_{app} (min^{-1})	Time (min)	Particle Size (nm)
AuNPs	0.36	14	24.1
AgAuNPs (2.0 ml Au)	0.52	8	75.2
AgAuNPs (5.0 ml Au)	0.62	5	55.2

AuCu-Pt

Catalysts with a AuCu metal core and Pt metal shell were synthesized.[47]

Synthesis of catalyst

- Oleylamine (OAm)-stabilized AuNPs were synthesized by dissolving 50 mmol $HAuCl_4$ in 4.6 ml oleylamine and removing O_2 with gaseous N_2. The solution was heated to 160℃ and stirred for 1 hr, then cooled to room temperature and precipitated by adding methanol. To synthesize AuCuNPs, a solution of $C_{10}H_{14}CuO_4$ in OAm was mixed with the AuNP solution, heated at 280℃ for 30 min with gaseous N_2 flow and stirring. After cooling to room temperature, AuCuNPs were precipitated out with methanol. The molar ratio of Au:Cu was 1:4. To synthesize the AuCu-Pt catalyst, $C_{10}H_{14}PtO_4$ was dissolved in OAm at 240℃ with N_2 and stirring for 1 hr. The solution was cooled down to room temperature and the catalyst precipitated out with methanol.

Characterization

- TEM analysis showed average diameters of AuNPs as 7.8 ± 1.5 nm, AuCuNPs as 8.3 nm, and AuCu-Pt as 9.1 nm.

Reduction Reaction

- Prior to each reaction, the catalyst was ultrasonicated for 15 min. The reaction was performed in a quartz cuvette, with 100 µl of 10 mM of the NPs added to 100 µl of 1mM 4-nitrophenol solution, adjusting the volume to 3.5 ml with water and 100 µl of 100 mM $NaBH_4$.

Reusability

- Reusability test was not performed.

Results

- K_{app}, reaction times and particle sizes of nanoparticles are compared in Table 6.

Table 6. K_{app}, reaction times and particle sizes of nanoparticles.

	K_{app} (min^{-1})	Time (min)	Particle Size (nm)
AuNPs	0.009 ± 0.0001	> 30	7.8
AgCuNPs	0.013 ± 0.0001	12	8.3
AgCu-PtNPs	0.039 ± 0.0002	10	9.1

AgAuPd

The catalytic activity of the hollow trimetallic AgAuPd nanocatalyst without polymer stabilizers was compared to AgAu bimetallic and monometallic catalysts.[48]

Synthesis of catalyst

- The following synthesis procedures are referenced and only described briefly in this review. Ag nanoparticles were synthesized by mixing $AgNO_3$ solution and $NaBH_4$ solution with citrate solution and water at 70℃ for 1 h, then cooled and diluted.[49,50] Au nanoparticles were synthesized by the citrate reduction method. $HAuCl_4$ solution in water was boiled, sodium citrate solution was added and stirred for 15 min until cooled, washed and diluted.[51] Pd nanoparticles were synthesized by dropping cooled ascorbic acid into cooled H_2PdCl_4 at 4℃, stirring for 30 min and diluted.[52]

  AgAu nanoparticles were synthesized by adding $HAuCl_4$ solution to NH_2OH*HCl solution and centrifuged for purification.[50]

  AgAuPd nanoparticles were synthesized by mixing H_2PdCl_4 solution to the preformed AgAu, dropping cooled ascorbic acid and stirred for 30 min, then centrifuged and diluted.[52]

Characterization

- UV-vis spectra, TEM and wavelength dispersive x-ray spectroscopy (WDS) analyses were obtained. The UV-Vis spectra showed the disappearance of the absorption peaks of Ag and

Au after the deposition of Pd nanoparticles because Pd does not display surface plasmon resonance in this range. WDS analysis confirmed the elemental composition of each catalyst.

Reduction reaction

- 1.275 ml of 15 mM $NaBH_4$ solution was mixed with 1.5 ml of 0.2 mM 4-nitrophenol solution in a quartz cuvette. 75 μl of 2.0 mM of catalyst was added to initiate the reaction, which was recorded for 20 min.

Reusability

- Reusability test was not performed.

Results

- k_{app} and average particle sizes are compared in Table 7. For the bi- and tri-metallic compositions, only the ratios with the highest catalytic performance are reported.

Table 7. k_{app} and average particle sizes of nanoparticles.

	k_{app} (min^{-1})	Particle Size (nm)
Ag	$1.2 * 10^{-3}$	18 ± 2
Au	$8.2 * 10^{-3}$	21 ± 2
Pd	$15.7 * 10^{-3}$	30 ± 3
Ag_2Au_1	$9.8 * 10^{-3}$	23 ± 2
$Ag_2Au_1Pd_2$	$46.6 * 10^{-3}$	32 ± 3

Table 8. Review of 4-nitrophenol reduction studies.

Metals	Support	Stabilizer	Avg. NP size (nm)	Reusability	k_{app} (min^{-1})	Notes	Ref.
Pd	Graphene	-	5.8	85% after 5 reuses	2.192	• Lower Pd content increased reactivity • Multi-substituted nitrophenols showed low reactivity • *o-* > *p-* > *m-*	(9)
AuPd	Graphene	-	3.46	91% after 3 reuses	0.867	• *k* significantly higher than Au/G (0.109) and Pd/G (0.164)	(41)
Ag	-	Calcium alginate	7	Constant after 3 reuses	$1.04*10^{-5}$	-	(43)
Au	-	Calcium alginate	5	Constant after 3 reuses	$0.17*10^{-5}$	-	(43)
Pt	-	PVPh	16	27% after 3 reuses	$1.12*10^{-2}$	• Pt-PVPh > bare Pt	(44)
AgAu	-	Sodium citrate	55.2	-	0.62	• AgAu > Au	(45)
AuCu-Pt	-	Oleylamine	9.1	-	0.039	• AuCuPt > AuCu > Au	(47)
AgAuPd	-	-	32	-	$46.6*10^{-3}$	• Pd > Au > Ag • AgAuPd > Pd > AgAu	(48)

2. Experimental

2.1 Reagents

Reagents used for catalyst preparation and nitrophenol reduction are listed in Table 9 with their molecular weight, purity and supplier.

Table 9. Table of reagents used for catalyst preparation and nitrophenol reduction.

Compound	**Molecular weight (g/mol)**	**Purity**	**Supplier**
Tetra chloroauric (III) acid trihydrate	393.83	99%	Sigma Aldrich
Poly(vinyl alcohol)	13000-23000	87-89% hydrolyzed	Sigma Aldrich
Polyvinyl pyrrolidone	29000	N/A	Sigma Aldrich
Polyethylene glycol	8000	N/A	Sigma Aldrich
Sodium borohydride	37.83	≥98.0%	Sigma Aldrich
Activated carbon SX1G	/	N/A	Norit
Biochar SWP700	/	/	UK Biochar Research Centre
4-nitrophenol	139.11	≥99%	Sigma Aldrich

2.2 Synthesis of Catalyst

The sol immobilization technique was used to synthesize supported Au nanoparticles. For 1 g of catalyst with a nominal metal loading of 1% wt, 0.0209 g of $HAuCl_4*3H_2O$ were dissolved in 0.3905 L of water. 0.643 ml of fresh aqueous PVA solution (0.1012 g in 10 ml of water stirred at 100℃ until dissolved and cooled) were added and stirred for 3 minutes. After 3 min, fresh aqueous $NaBH_4$ solution (0.0096 g in 2.5 ml of water) was added to obtain a dark red color. After 30 minutes of stirring, 0.99 g of AC was added and the pH adjusted to 2 with concentrated H_2SO_4. The reaction was left to stir at RT for 1 h and filtered using a Buchner funnel and two filter papers. The slurry was washed with water until it reached neutral pH. The catalyst was dried overnight at RT, then in an oven at 80℃ for 4 h. The synthesis procedure is shown on Figure 9.

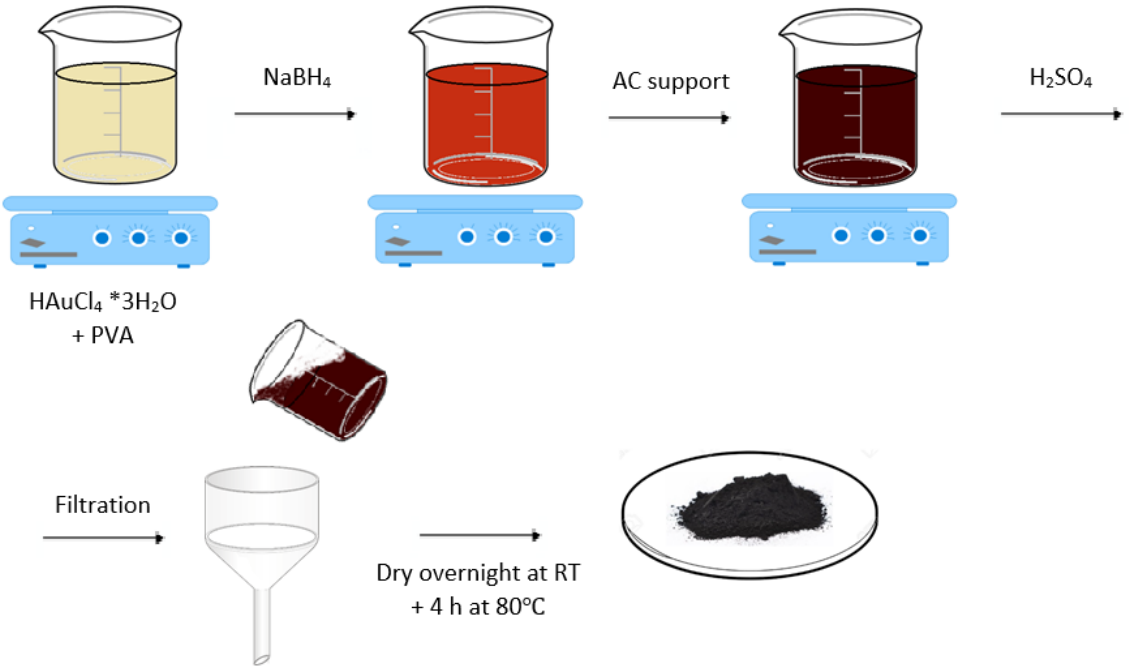

Figure 9. Sol immobilization procedure for gold nanoparticle catalyst synthesis.

2.3 Biochar support as replacement for AC

A biochar sample was tested as a support for the catalyst in place of activated carbon. The feedstock material of the biochar was soft wood pellets, with a pyrolysis temperature of 700℃ and a mean total surface area of 162.3 m^2/g as opposed to 1049 m^2 of AC. This specific sample contained 90.21 wt% in C, 6.02 wt% in O, 1.83 wt% in H, 1.00 wt% moisture, as well as small amounts of N. The procedure for catalyst synthesis using biochar was similar to the standard experimental procedure using AC except for the amount of the PVA solution added (PVA 0, PVA 0.05 and PVA 0.1 instead of PVA 0.65 as with the AC catalyst) and stirring of the final pH adjusted solution for 4 h instead of 1 h. The PVA amount was varied to study the effect of PVA amount in terms of the final particle size of Au and the effectiveness of adsorption of preformed gold nanoparticles on the support and dispersion of the supported gold nanoparticles.

2.4 Characterization of catalysts

Several analytical techniques are employed in the characterization of the nanoparticle catalysts. The techniques used in this study are:

- UV-Visible Spectroscopy (UV-Vis)
- Dynamic Light Scattering (DLS)
- X-ray Diffraction (XRD)
- Transmission Electron Microscopy (TEM)

2.4.1 UV-Visible Spectroscopy

UV-visible spectroscopy is a commonly used analytical technique in observing and quantifying electronic transitions of molecules. In metal ions, electronic transitions occur when photons excite electrons to a higher energy orbital. To move an electron from one energy orbital to another, the energy of the photon must be equal to the energy gap between the two orbitals. This energy of the photon is within the electromagnetic range of ultraviolet (UV) or visible, hence the name UV-visible spectroscopy.

A deuterium lamp for the ultraviolet range of 190-400 nm and a tungsten filament for the visible range of 350-2500 nm are used as the irradiation source. A monochromator separates the radiation, thus only irradiating the sample with the desired wavelength of radiation.

To confirm the formation of gold metal nanoparticles from $AuCl_4^-$, UV-Vis analysis can be performed following the formation of the Au colloidal solution prior to the addition of the support. $AuCl_4^-$ in solution displays peak absorbance at 222 nm, whereas metallic Au colloidal nanoparticles display peak absorbance at 490-520 nm. Factors that influence peak position,

intensity and width include the size, shape, concentration, aggregation of particles, as well as dielectric properties of the chemical environment which can change with solvent and stabilizer. The UV-Vis technique provides only an approximate of the NP dimensions and is used to support other analytical techniques more suitable for quantitative analysis. The spectrophotometers used were the Perkin Elmer UV-VIS-NIR Lambda 19 and the Varian Cary 1E UV-Visible.

2.4.2 Dynamic Light Scattering (DLS)

Dynamic light scattering (DLS) is a technique used to determine the size distribution of particles in solution. A monochromatic light reaches the sample in which the particles are moving in Brownian motion. Particles with sizes smaller than the wavelength of the incident light scatter the light in all directions. The scattered light is projected onto a screen showing speckles of light and dark. The light areas are areas of constructive interference, while the dark areas represent destructive interference. Fluctuations in intensity over time create a scattering pattern, which allows for the analysis of the size distribution of the particles (Figure 10). DLS analysis was carried out using a Malvern Zetasizer Nano ZS.

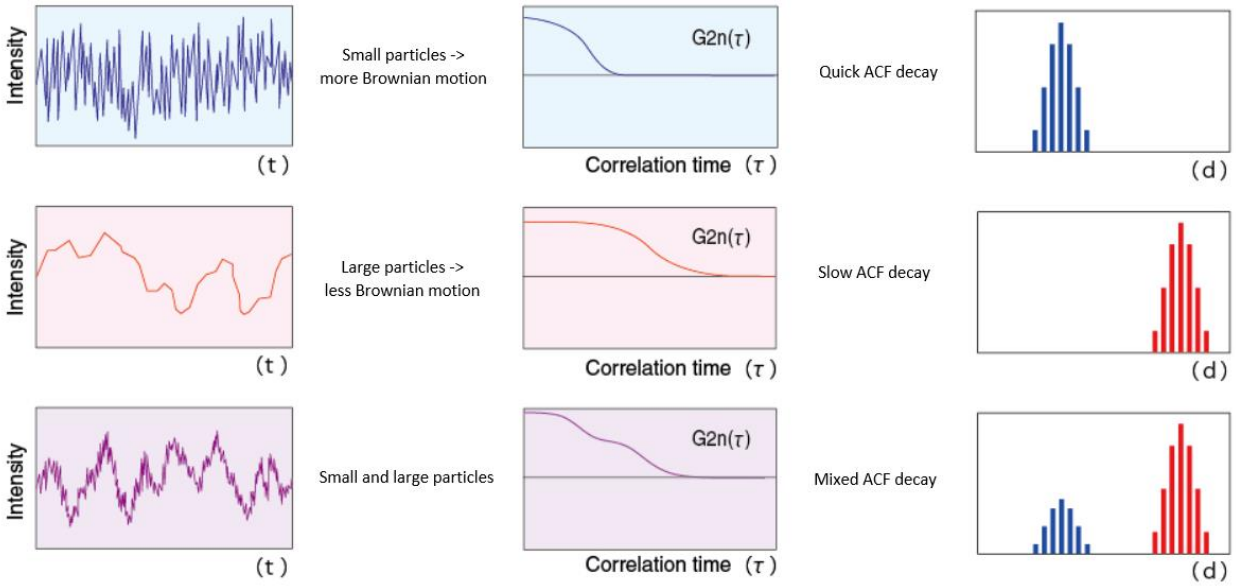

Figure 10. Scheme of a DLS analysis. Particle size distribution is obtained from the graph of auto-correlation function (ACF) in the time domain.

2.4.3 X-ray Diffraction (XRD)

X-ray diffraction (XRD) is used to obtain information regarding unit cell structure and crystal size of a solid. Electrons vibrating in an electric field backscatter incident X-ray light. Bragg's law is the theoretical basis of X-ray diffraction. Within a crystalline solid consisting of planes, incident X-ray is reflected. When the X-ray reflected by the lower plane, given by nλ, and that reflected by the upper plane, given by 2dsinθ, are in phase there is constructive interference resulting in a diffraction pattern. Bragg's law is given by:

$$2d\sin\theta = n\lambda$$

where d = distance between planes, θ = angle between the plane and incident X-ray, n = positive integer, and λ = wavelength of the incident X-ray.

The resulting diffractogram plots the peak intensity against θ. The width of the peaks can be used to analyze crystal size. Broader peaks signify smaller crystallite sizes due to increased strain within the solid. To accurately determine the crystallite size, the Scherrer equation is used:

$$B(2\theta) = K \lambda / L\cos\theta$$

where B = peak width, K = Scherrer's constant, and L = crystallite size (Figure 11).

The peak width B is taken as the FWHM (full width at half maximum) of the peak.

XRD analysis was performed on the AuNPs after the immobilization step of the synthesis. Metallic gold has an FCC crystalline structure. The (111) Au plane with a strong diffraction peak at 38.2° 2θ was used to calculate crystallite size. A Bragg-Brentano X'pertPro Panalytical X-ray diffractometer was used with a copper anode (K_α radiation at λ = 1.5418 Å) as the X-ray source with a 0.08° step size and acquisition time of 1300 s/step in 36 - 41 2θ range. Activated carbon diffraction was also analyzed for overlapping peaks at the peak range of interest.

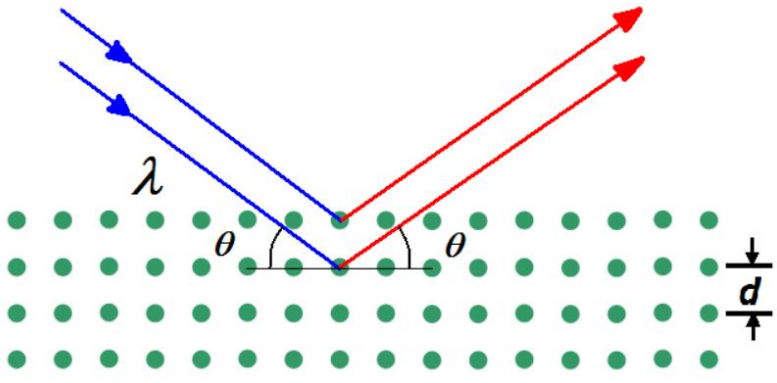

Figure 11. X-ray diffraction scheme on a crystal lattice.

2.4.4 Transmission Electron Microscopy (TEM)

Transmission electron microscopy (TEM) is a high-resolution microscopy technique used to observe a sample with an electron beam. The high resolution compared to optical microscopy

comes from the higher energy, or smaller wavelength, of the electrons. TEM is used on samples usually less than 100 nm in thickness. The microscope is composed of the electron source, the lens system with a vacuum pipe through which the electron beam passes, the sample holder, and the imaging system which includes a series of electromagnetic lenses and electrostatic plates. The electron beam is adjusted by manipulating the lenses and plates.

Although XRD analysis provides an estimate of the Au crystallite dimensions, TEM is the most precise method for determining the average nanoparticle size and particle size distribution. Au nanoparticles supported on AC and on biochar were characterized by TEM analysis. Samples were suspended in ethanol and treated with ultrasound for 15 minutes. The suspension was deposited on a quantifoil-carbon film supported by a Cu grid and dried at 100°C. The TEM/STEM FEI TECNAI F20 microscope at 200 keV was used for observations. Over 400 nanoparticles under the size of 13 nm were analyzed to obtain the particle size distribution.

2.5 Analytics

2.5.1 UV-Vis spectroscopy

To trace the kinetics of the reduction reaction of the Au precursor and the formation of the plasmon peak, absorbance is measured as a function of time. UV-Vis spectroscopy is an analytical technique for identification and quantification of compounds such as transition metal ions, conjugated organic compounds and biological macromolecules. Absorption or transmission/reflection can be measured in the ultraviolet and visible ranges of the electromagnetic spectrum. In the visible range, the absorption of light is directly correlated with the visualized color of the sample. Absorptions measure electronic transitions from the ground state to the excited state. When a molecule absorbs a specific quantity of energy in the form of ultraviolet or visible light, electrons are excited to higher molecular orbitals. The measured absorbance is directly

proportional to the concentration of the absorbing compound in the sample according to the Beer-Lambert law:

$$A = \varepsilon * l * c$$

where A = absorbance, ε = molar extinction coefficient (in M^{-1} cm^{-1}), l = optical path length (cm), and c = concentration of the absorbing compound in solution. The molar extinction coefficient measures the probability of the electronic transition. The optical path length in the UV-Vis instrumentation is the width of the cuvette through which the incident light travels. Considering the factors that define absorbance, A can be defined and written in terms of the intensities of incident and transmitted light:

$$A = \log_{10}(I_0/I)$$

where I_0 = intensity of incident light and I = intensity of transmitted light.

The molar extinction coefficient of 4-nitrophenol for each UV-Vis spectrophotometer used was obtained by calibration. 4-nitrophenol solutions of different concentrations ($1.5*10^{-4}$M, $1.0*10^{-4}$M, $5.0*10^{-5}$M, $2.0*10^{-5}$M, $1.0*10^{-5}$M) with $4.5*10^{-3}$M in $NaBH_4$ were analyzed on each instrument. The absorbance at 400nm for each solution was plotted against the concentration, and the obtained slope of the line was taken as the molar extinction coefficient. An average coefficient value of three sets of calibrations was taken.

2.6 4-nitrophenol reduction reaction

The reduction of 4-nitrophenol by sodium borohydride to 4-aminophenol is a model reaction for observing catalytic activity because it does not proceed without a catalyst. Both 4-nitrophenol and $NaBH_4$ adsorb onto the active sites on the AuNPs to react (Figure 12). Therefore, a higher concentration of 4-nitrophenol implies a lower rate constant as there is less $NaBH_4$ adsorbed onto

the NPs to react. In this reaction, the $NaBH_4$ supply is in excess with respect to 4-nitrophenol to maximize the rate constant (Figure 13). This reaction can, therefore, be seen as a pseudo first-order reaction.

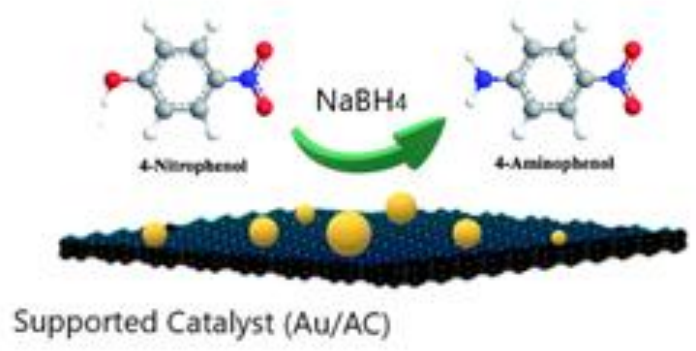

Figure 12. 4-nitrophenol conversion to 4-aminophenol with supported catalyst.

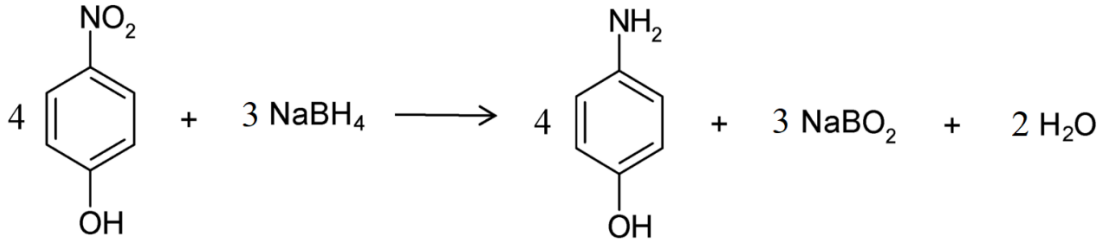

Figure 13. Stoichiometric reaction scheme of 4-nitrophenol reduction to 4-aminophenol.

2.7 Kinetics

To test the activity of the AuNPs, the reduction of 4-nitrophenol by $NaBH_4$ in water was analyzed using UV-Vis. Repeated measurements of the reaction solution were taken either manually or automatically by the instrument depending on the reaction setup. The peak around 400 nm, labeled 4-NP in Figure 14, represents the absorbance of 4-nitrophenol. This peak is seen disappearing over

time, while a new peak around 300, labeled 4-AP which represents 4-aminophenol, gradually emerges over time. The noise peaks seen around 200-280 nm are from the change of filter. The changes in absorbance values for 4-nitrophenol were used in the Beer-Lambert law to calculate its concentration. The calibrated molar extinction coefficient for the UV-Vis was $\varepsilon = 18100 M^{-1} cm^{-1}$.

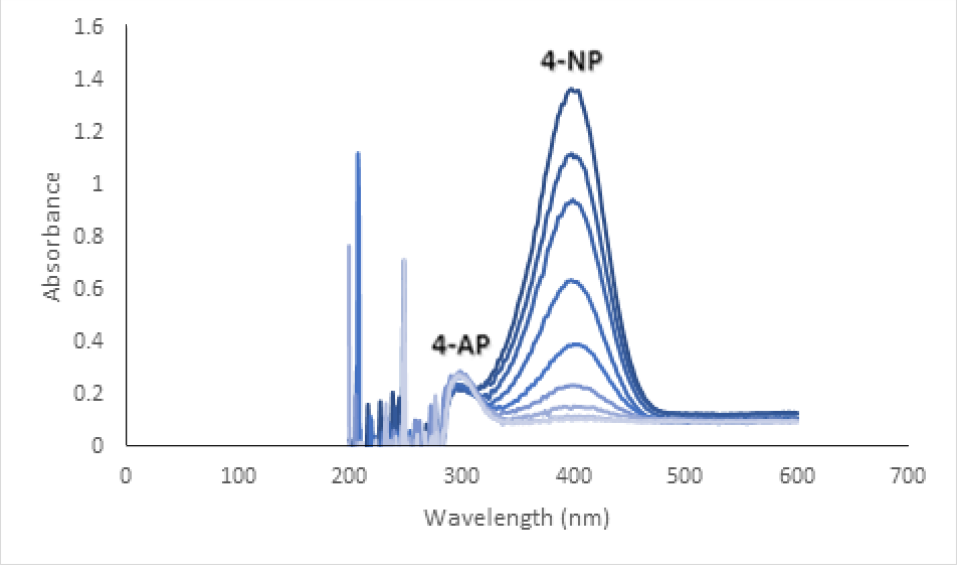

Figure 14. 4-nitrophenol peak disappearance and 4-aminophenol peak emergence over reaction time.

2.8 Preparation of reaction solutions

A 0.01 M 4-nitrophenol stock solution was prepared by dissolving 0.1391 g of 4-nitrophenol in 100 ml of water in a volumetric flask. Fresh 4-nitrophenol reaction solutions ($2.0*10^{-4}$ M) were made from this stock solution by micropipetting 500 μl of the stock solution into a 25 ml volumetric flask and diluting to the mark with distilled water. To prepare the $NaBH_4$ solution ($9.0*10^{-3}$ M) with a 4-nitrophenol:$NaBH_4$ molar ratio of 1:45, 8.5 mg of $NaBH_4$ were dissolved in water, transferred into a 25 ml volumetric flask and diluted to the mark with water. 4.0 mg of the catalyst were weighed out on an analytical balance. The blank solution was prepared by dissolving

4.3 mg of $NaBH_4$ in water, transferring into a 25 ml volumetric flask and diluting to the mark with water.

2.9 Effect of reaction setup

2.9.1 Stirring (round-bottom flask) setup

25 ml of 4-nitrophenol ($2.0*10^{-4}$M) solution was poured into a 250 ml round-bottom flask with stirring at 1000 rpm at room temperature. 25 ml of $NaBH_4$ ($9.0*10^{-3}$M) solution was then added to the flask to yield a yellow color, and the catalyst was added lastly, starting the timer to record the reaction time (Figure 15). While stirring, each measurement was taken by sampling 3.5 ml of the solution using a syringe with a 0.22 μm PTFE filter to filter out the catalyst. The filtered sample was analyzed by UV-Vis in a 1 cm quartz cuvette. The reference sample, the $NaBH_4$ solution, was analyzed simultaneously in the reference sample holder. A sample was filtered and analyzed approximately every 4 minutes, and the analyzed sample was discarded.

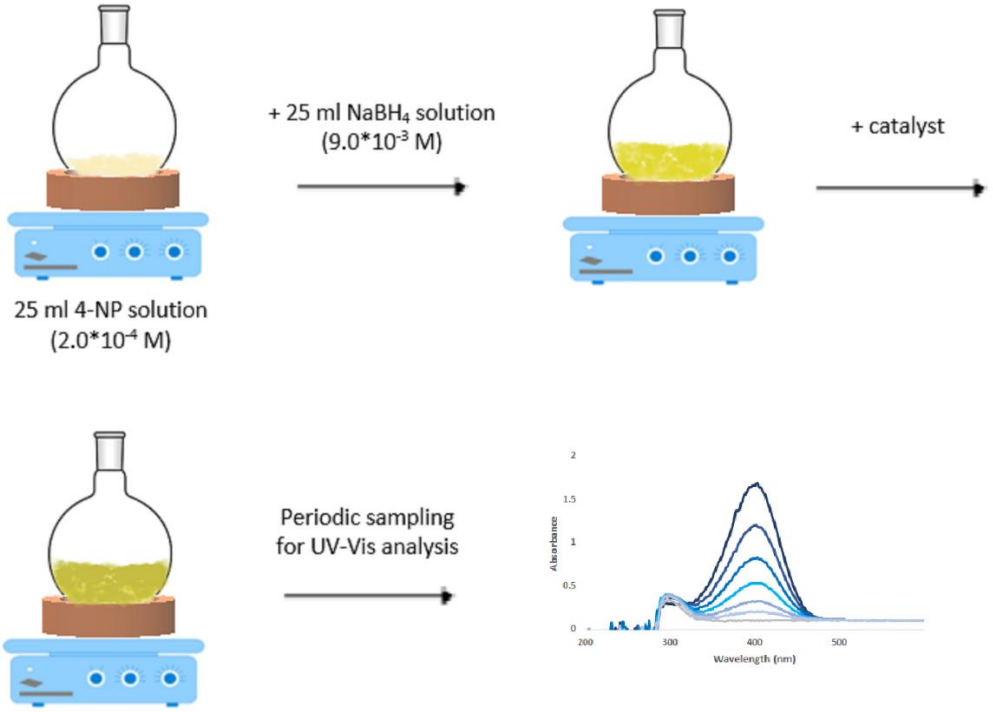

Figure 15. Stirring reaction setup and procedure.

2.9.2 Non-stirring (cuvette) setup

The catalyst was put in a 50 ml beaker and the 25 ml of 4-nitrophenol ($2.0*10^{-4}$M) solution added. 25 ml of the $NaBH_4$ ($9.0*10^{-3}$M) solution was then added, starting the timer to mark the start of reaction. The yellow solution was gently mixed using a pipette motion, making sure the catalyst has had a chance to evenly distribute itself before sampling, while avoiding any aggressive stirring. A sample was drawn into a quartz cuvette and analyzed 2 minutes and 30 seconds into the start of the reaction (Figure 16). Measurements were taken of the same sample approximately every 3 minutes until the end of the reaction which is marked by the disappearance of the 4-nitrophenol peak at around 400 nm. The reference sample, the $NaBH_4$ solution, was analyzed simultaneously in the reference sample holder.

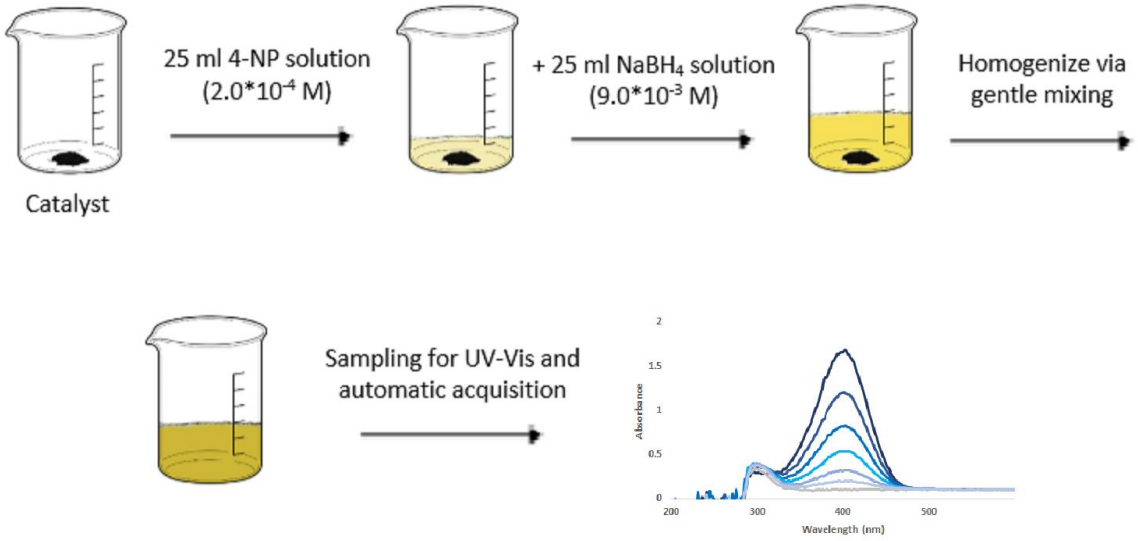

Figure 16. Non-stirring reaction setup and procedure.

2.10 Catalyst Reusability

Recovery and reusability of the catalyst using PEG as stabilizer were tested for 5 cycles with the non-stirring method. After each reaction, the catalyst was recovered from the aqueous solution by centrifugation at 4500 rpm for 15 min. The supernatant was removed, and the catalyst was recovered using 25 ml of 4-nitrophenol solution ($2.0*10^{-4}$M). This solution mixture was reacted with 25 ml of $NaBH_4$ solution ($9.0*10^{-3}$M) and its reaction traced.

2.11 Effect of 4-nitrophenol:$NaBH_4$ molar ratio

This reaction involves $NaBH_4$ in excess with respect to 4-nitrophenol, with a 4-nitrophenol:$NaBH_4$ ratio of 1:45. Therefore, the reaction follows a pseudo-first order kinetics. However, considering the possibility of degradation of the hygroscopic $NaBH_4$ in solution during reaction, tests were

performed with increased amounts of $NaBH_4$. The 4-nitrophenol:$NaBH_4$ ratios of 1:60, 1:70 and 1:80 were tested.

2.12 Stability of 4-nitrophenol and $NaBH_4$ solutions

The long-term stability of the two reactant solutions was tested to ensure accurate comparisons of reactions over an extended period. For each reaction, a fresh sodium borohydride solution is made. Solutions were prepared from one old and one new lot of sodium borohydride. The reaction rate constant, *k*, for each trial was measured and compared.

2.13 Stability of catalyst

Long-term stability of the catalyst was tested by comparing the activities of a newly prepared catalyst with an old catalyst which was approximately 1 year old. The difference between the two catalysts is in the amount of stabilizer. The old catalyst had a PVA to Au ratio of 0.6, whereas the new catalyst had a ratio of 0.65.

3. Results and Discussion

3.1 UV-Vis

With the UV-Vis spectra of the Au precursor and the AuNP colloidal solution, it is possible to study the formation of the nanoparticles during synthesis. Although the position and shape of the plasmonic peak of the AuNPs can provide an estimate of their dimensions, other techniques such as XRD and TEM are necessary for an accurate determination of crystallize size and average dimension.

Figure 13 shows UV-Vis spectra of the Au precursor and the colloidal solution with a PVA:Au weight ratio of 0.65. At around 300 nm, the precursor shows a peak corresponding to the yellow color of the solution. At 3 min after having added the $NaBH_4$, the plasmonic peak of the AuNPs shows around 500 nm. With time, a shift in this plasmonic peak to a higher wavelength (red-shift) indicates an increase in nanoparticle size. Conversely, a shift to a lower wavelength (blue-shift) indicates a decrease in nanoparticle size. The exact position of the peak as well as its intensity and width depend on many factors such as the size, shape, concentration or aggregation of the nanoparticles. In Figure 17, a slight shift of the plasmonic peak to a higher wavelength can be seen after 30 minutes. From 30 to 120 minutes, there is no increase in wavelength seen, indicating the nanoparticles are stable after 30 minutes.

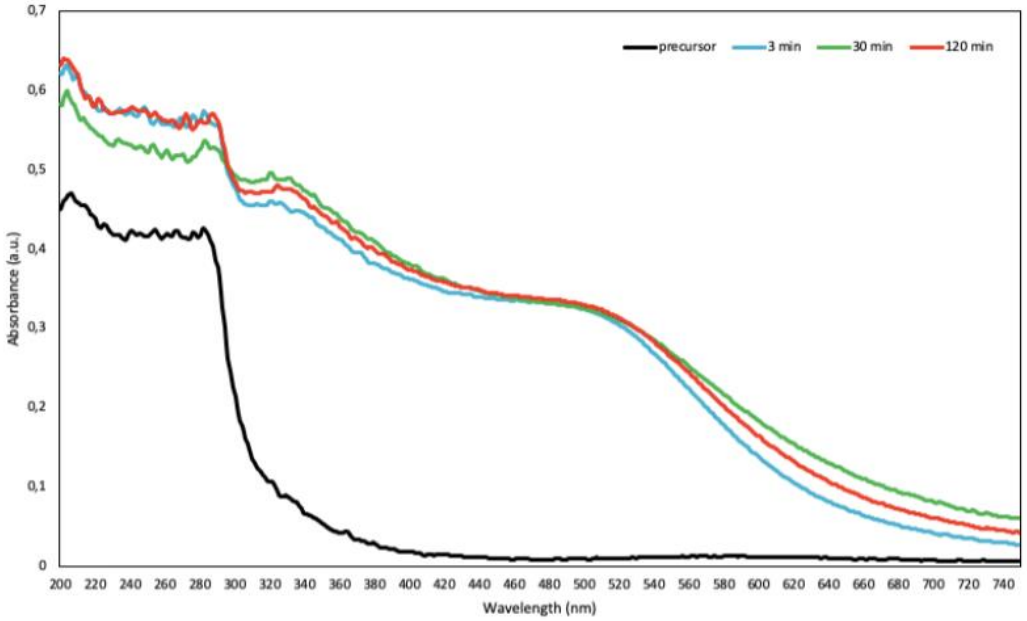

Figure 17. UV-Vis spectra of Au colloidal solution with PVA 0.65 before and after the addition of $NaBH_4$.

The same analysis was performed for the colloidal solutions with PVA:Au weight ratio of 0.1 and 0.65 (Figure 18). From 3 to 25 min after the addition of $NaBH_4$, a shift and change of shape of the

plasmonic peak is shown for both. However, the degree of this shift and change over time is greater in the PVA 0.1 colloidal solution, indicating that a higher amount of PVA leads to the formation of more stable nanoparticles.

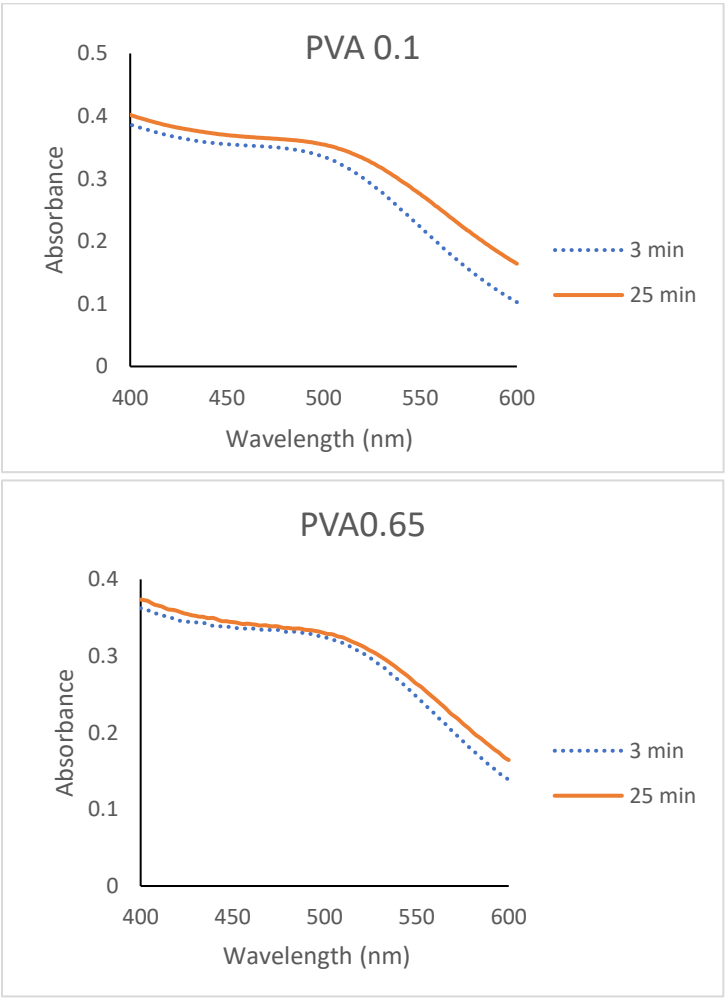

Figure 18. UV-Vis spectra of Au colloidal solutions with PVA 0.1 and PVA 0.65 after 3 min and 25 min from the addition of $NaBH_4$.

3.2 Dynamic Light Scattering (DLS)

To evaluate the stability of the nanoparticles over time, the change in the hydrodynamic diameter as a function of time was observed. The hydrodynamic diameter of the AuNPs stabilized with PVA in solution was previously analyzed using DLS. The solution was analyzed after the reduction by

$NaBH_4$ for five measurements in total to trace the stability of the nanoparticles: after 30 minutes, 1.5 h, 24 h, 48 h, 120 h (Figure 19). There was an initial decrease in the first 24 hours from 5.6 nm at 30 minutes to 4.2 nm at 24 h, likely due to the polymers initially bonding and thinning around the nanoparticles. NP size remained constant after 120 hours of formation.

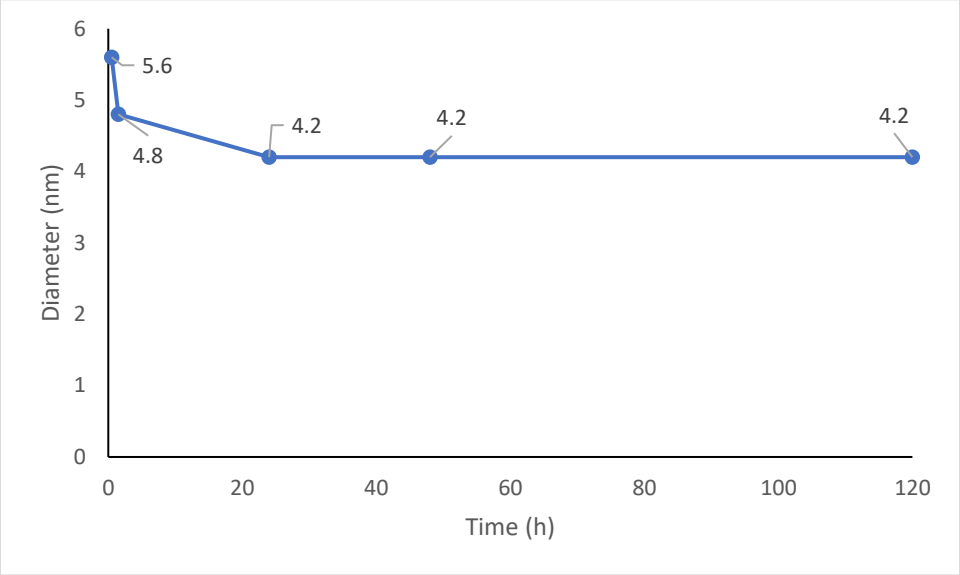

Figure 19. Average size of Au/AC stabilized with PVA 30 min, 1.5 h, 24 h, 48 h and 120 h after reduction.

3.3 X-Ray Diffraction (XRD)

The UV-Vis and DLS analysis can give an idea about the dimension and stability of the preformed Au nanoparticles; however, the immobilization step during synthesis could affect the final dimension. To evaluate the AuNP dimension after immobilization, XRD analysis allows for an accurate determination of the crystallize size with the Scherrer equation. In Figure 20 the diffraction peak of Au/AC PVA0.65 was compared with those of the series of catalysts prepared with biochar as support (Au/Bioc PVA 0, Au/Bioc PVA 0.05 and Au/Bioc PVA 0.1). Moreover, the XRD pattern of the supports (AC and biochar) were reported to evaluate any possible overlap. From Figure 20 it is seen that the average NP sizes of the Au/biochar are larger than those of the Au/AC PVA0.65 catalyst, which is expected due to the higher amount of PVA presence in the

sample supported on active carbon. The presence of PVA results in a smaller crystallite size. Among the Au/biochar catalysts, the correlation between the amount of PVA added and average NP size is shown. Au/biochar PVA 0.05 and Au/biochar PVA 0.1 show little difference in NP size, whereas Au/biochar PVA 0 displays significantly higher average NP size.

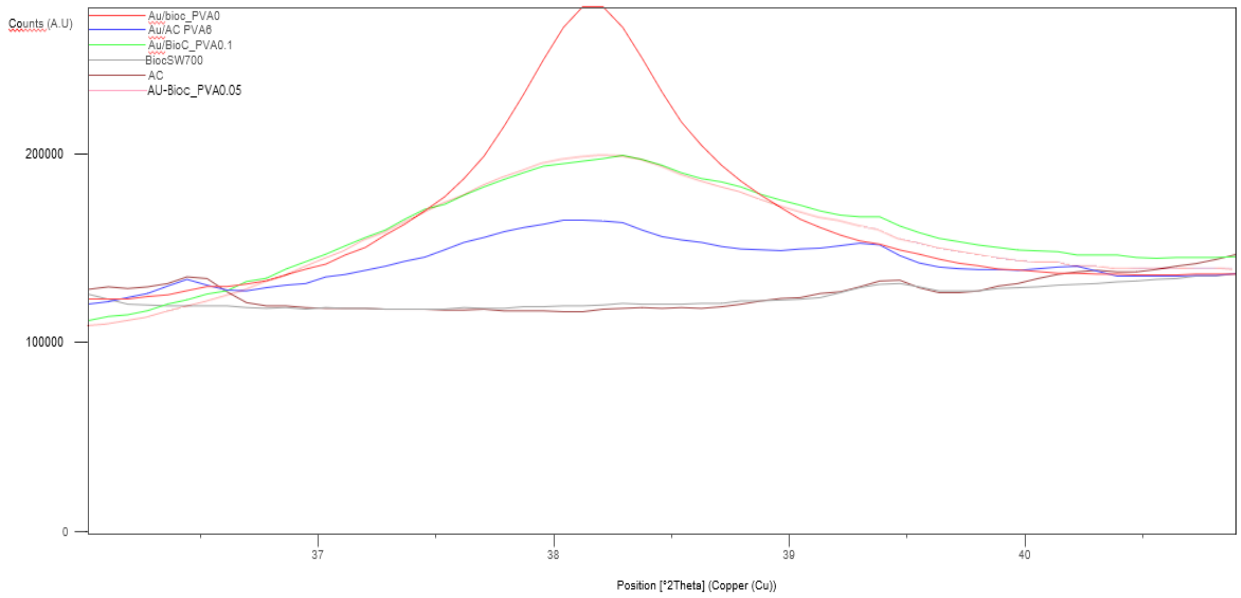

Figure 20. X-ray diffraction pattern of supports and catalysts. Red: Au/biochar PVA 0; blue: Au/AC PVA 0.65; green: Au/biochar PVA 0.1; grey: biochar; brown: AC; pink: Au/biochar PVA 0.05.

3.4 Transmission Electron Microscopy (TEM)

For a proper comparison of the effect of the amount of PVA and of the support on the mean Au nanoparticle size, TEM analysis is required. For Au/AC PVA 0.65, the average particle size was 2.43±1.6 nm (Figure 21). For Au/AC without PVA, the average particle size was 8.86±11.5 nm (Figure 22). For Au/biochar without PVA, the average particle size was 5.84±2.3 nm (Figure 23). Results are summarized in Table 10.

The Au/AC without PVA showed a larger average particle size and particle size distribution compared to Au/AC PVA 0.65. The Au/biochar without PVA showed a smaller average particle size and particle size distribution compared to Au/AC without PVA. Some agglomeration of

particles of individual sizes in the range of 3-50 nm to yield a total agglomerate of over 100 nm was seen (Figure 24). In HAADF-STEM images, the intensity contrast resulting from differences in atomic number of the Au and the carbon in biochar enables a better distinction of the nanoparticles dispersed on the support. In the absence of the stabilizer, the biochar led to the formation of smaller nanoparticles.

Table 10. Mean AuNP sizes and standard deviation for catalyst with different supports and amount of PVA.

	Au/AC PVA 0.65	**Au/AC PVA 0**	**Au/Bioc PVA 0**
AuNP size	2.43±1.6	8.86±11.5	5.84±2.3

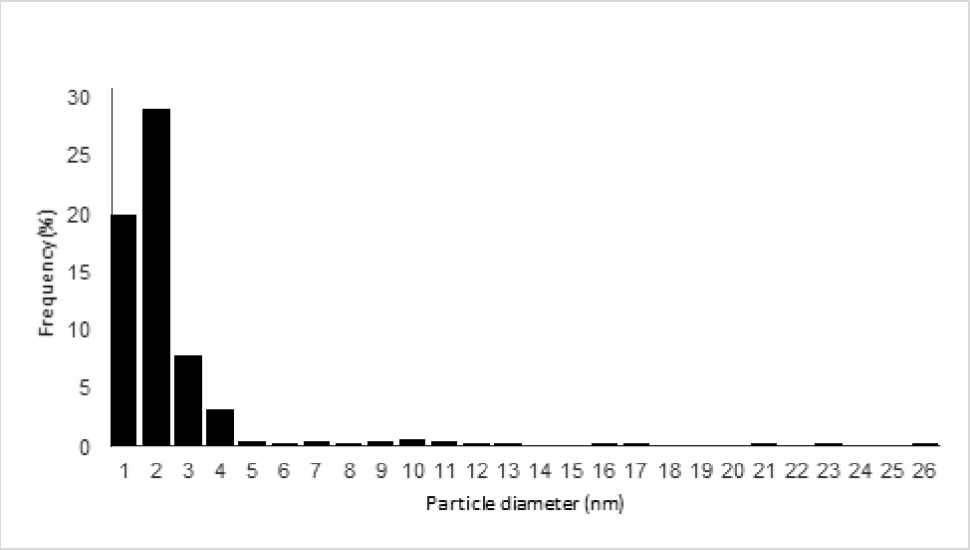

Figure 21. Mean particle size and particle size distribution of Au/AC PVA 0.65.

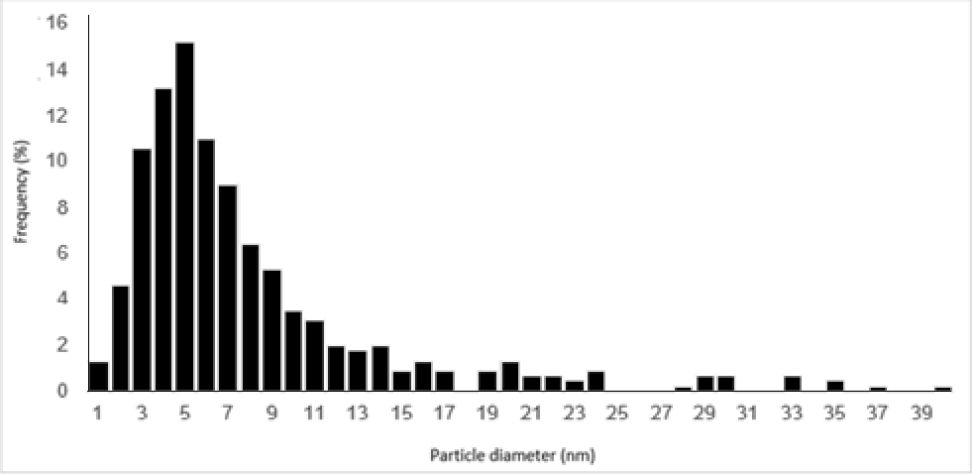

Figure 22. Mean particle size and particle size distribution of Au/AC PVA 0.

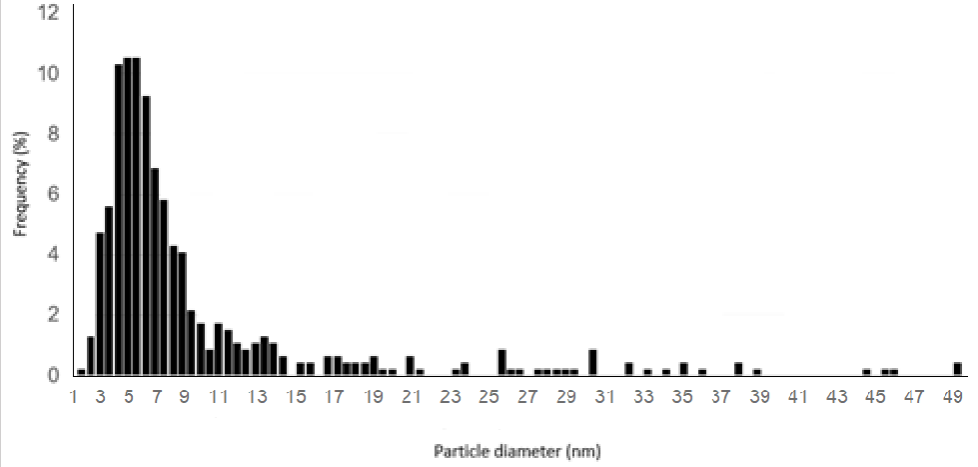

Figure 23. Mean particle size and particle size distribution of Au/biochar PVA 0.

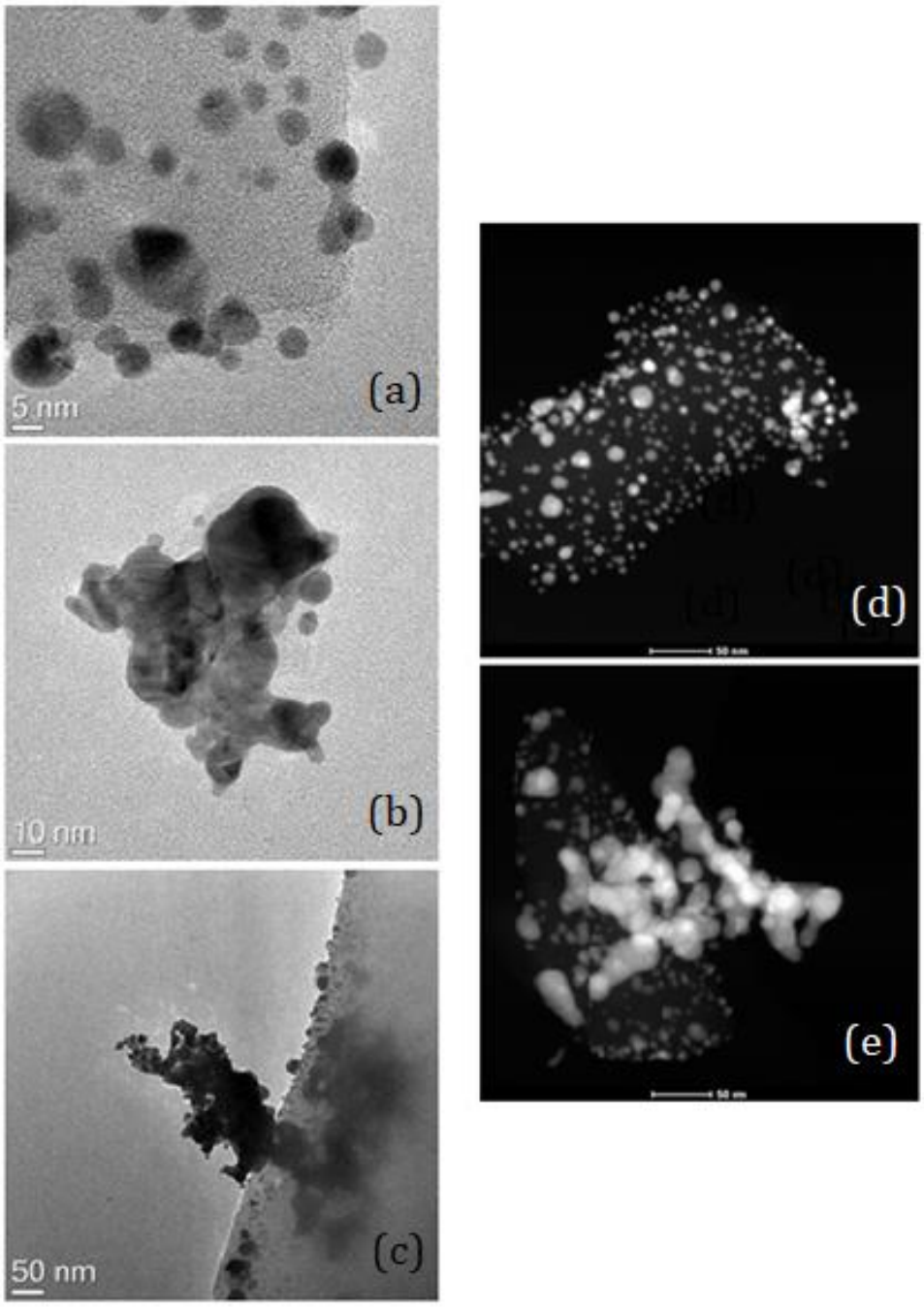

Figure 24. TEM and STEM-HAADF images of Au/biochar PVA 0. (a) Minimum dimensions of well-dispersed particles: 2.5 nm with agglomerates of <50 nm. (b) Agglomerates of particles 5-50 nm for a total of 80-90 nm. (c) Agglomerates of particles for a total of 290 nm. (d) Well-dispersed particles of 3-35 nm. (e) Agglomerates of particles 3-50 nm.

3.5 Stability of 4-nitrophenol solution

As reported in Chapter 2, fresh 4-nitrophenol solutions used for each reaction are dilutions of a stock solution. To check the stability of 4-nitrophenol, an old stock solution, prepared approximately 4 months prior, was tested against a newly prepared stock solution. The lot of 4-nitrophenol reagent used was the same for both stock solutions. Table 11 gives the *k* obtained using the two different stock solutions, and the old 4-nitrophenol solution shows a higher *k* as well as a lower maximum absorbance. With the assumption that $NaBH_4$ is in excess in the reaction, which holds true based on the final conversion rate for all reactions being 95%, it is expected that the reactions using the old 4-nitrophenol solution would exhibit a higher rate constant. The degradation of 4-nitrophenol in solution over time could explain the lower amount of 4-nitrophenol reacting with the same amount of catalyst, giving a higher *k*.

Table 11. *k* values for reactions using old vs. new 4-nitrophenol solutions.

Sample	***k* (min^{-1}) ±SD**
Old 4-NP sol'n	0.136±0.002
New 4-NP sol'n	0.0838

3.6 Stability of $NaBH_4$ as reagent

$NaBH_4$ solutions for each reaction are freshly prepared from one lot or container of $NaBH_4$. It is known that $NaBH_4$ is hygroscopic, and with time the water absorbed can reduce the reactivity. To evaluate the effect of this phenomena, $NaBH_4$ solutions prepared from a 6-month old vs. newly opened lot of $NaBH_4$ were compared to check for its stability. Table 12 shows that the old $NaBH_4$ resulted in a lower *k* with a high standard deviation, different from the new $NaBH_4$. The hygroscopicity of the $NaBH_4$ may have led to $NaBH_4$ molecules that are less active, especially at the surface of the container from which the $NaBH_4$ was sampled.

The stability tests performed on the two reactants highlight the importance of preparing fresh solutions with fresh lots of chemicals due to their possibility of skewing experimental data over time.

Table 12. Average *k* value and standard deviation for reactions using old vs. new lot of $NaBH_4$.

Sample	***k* (min^{-1}) ±SD**
Old $NaBH_4$	0.10±0.02
New $NaBH_4$	0.136±0.002

3.7 Stability of Catalyst

Two catalysts, Au/AC PVA 0.6 prepared approximately one year prior, and the newly prepared Au/AC PVA 0.65 were tested to compare the long-term stability of the catalyst. Figure 25 shows the superior performance of the newly prepared catalyst with a *k* value of 0.0794 vs. 0.0442 min^{-1}. Based on the correlation of *k* values of catalysts with different amounts of stabilizer, as previously researched in our lab and shown in Table 13, it is highly unlikely that this difference in performance is due to the slight difference in the amount of stabilizer. Following this trend, it is plausible to assume a significant decrease in catalytic activity over time.

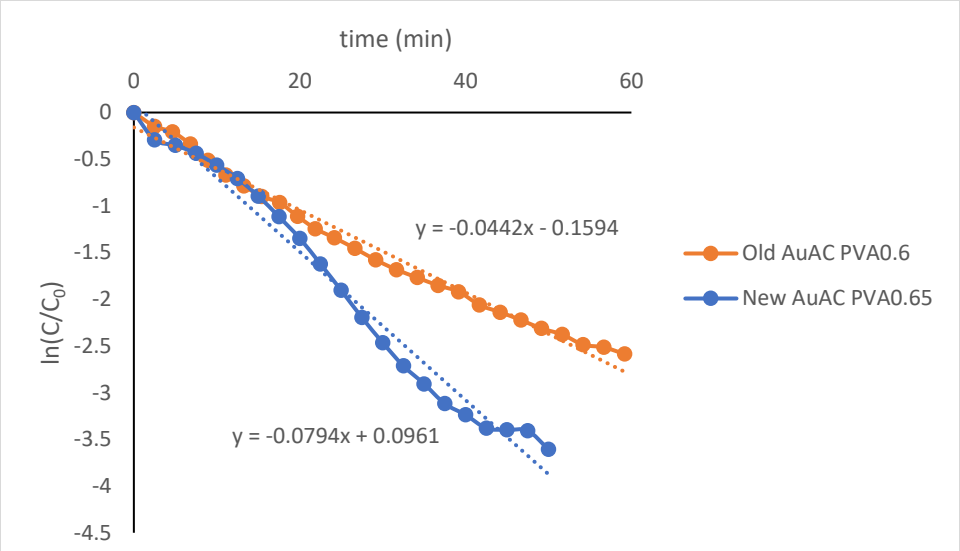

Figure 25. Reaction rate constants *k* for old vs. new catalyst.

3.8 Effect of 4-nitrophenol:$NaBH_4$ molar ratio

After the evaluation of the stability of all reagents and catalyst, some reaction parameters were investigated. Conversions of 4-nitrophenol with various molar ratios of 4-nitrophenol:$NaBH_4$ were compared. Although the 4-nitrophenol:$NaBH_4$ ratio of 1:45 is stoichiometrically in high excess, higher amounts of $NaBH_4$ were tested for any differences. As shown in Figure 26, there is a pattern of increased rate of conversion with higher amounts of $NaBH_4$ in solution. A pseudo-first order reaction is one which its kinetic rate depends on one reactant due to the excess of the other. Although $NaBH_4$ is added in stoichiometric excess, the data suggest there is a degradation of $NaBH_4$ occurring during the reaction. Further experiments should be done with increased amounts of $NaBH_4$ to see where a plateau occurs, then the reaction can be analyzed as a pseudo-first order reaction.

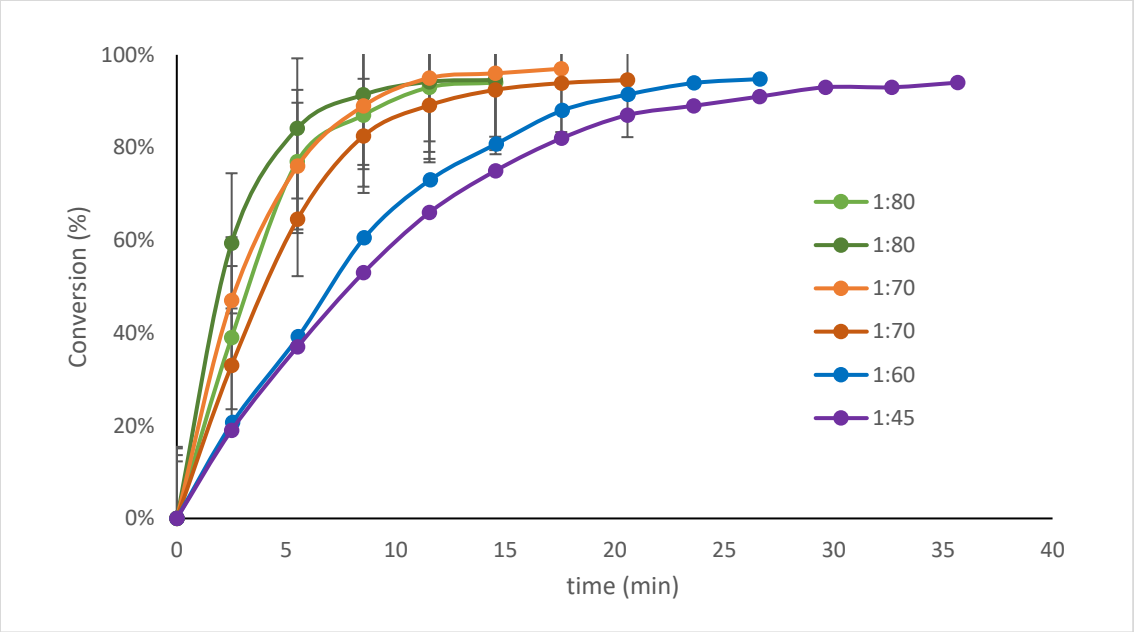

Figure 26. 4-nitrophenol conversion with various 4-nitrophenol:$NaBH_4$ ratios. Error bars represent standard error.

3.9 Polymer stabilizers

Because the reactions take place on the surface of the nanoparticles, slight changes in structure, size or chemical composition of the NPs can greatly alter catalytic properties. The high surface energy of nanoparticles also makes them thermodynamically unstable and, thus, nanoparticles tend to stabilize themselves through agglomeration and aggregation. A fine balance between increasing the surface area of the nanoparticles and maintaining their stability by avoiding aggregation must be kept. Too large of the nanoparticle size can hinder reactivity due to less surface area, and too small of the size can increase their surface energy, promoting aggregation. To prevent this, polymers with high chemical stability, solubility and non-toxicity are added as a stabilizing agent in synthesizing the catalyst. Stabilization by polymers occurs sterically, where the polymeric chains on the surface of the nanoparticles prevent their attraction and agglomeration. The presence of polymers, therefore, increases the stability of the nanoparticles to maintain their catalytic activity. Electrostatic stabilization is also possible, although the sensitivity of electrostatic forces

to ionic strength and pH changes makes them less desirable. Figure 27 shows gold nanoparticles stabilized using PVA and citrate that keep the nanoparticles from attracting each other.

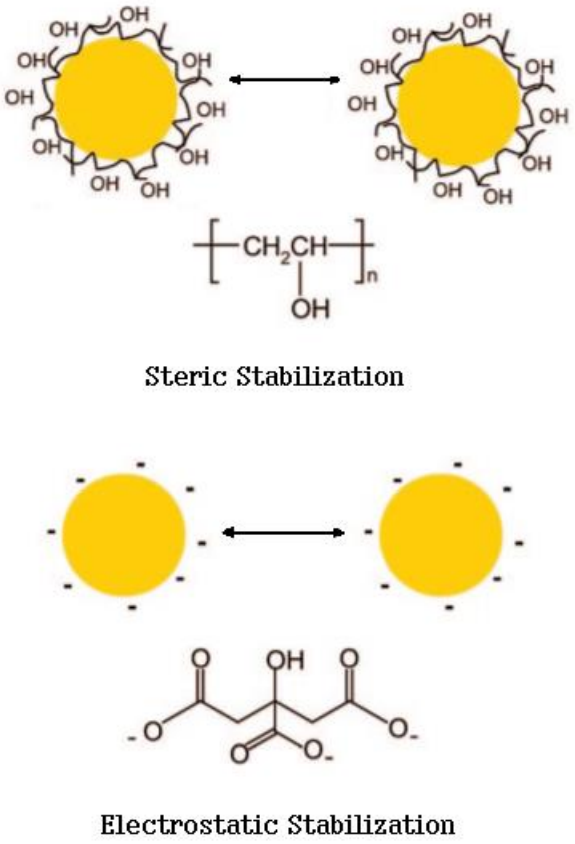

Figure 27. Scheme of steric vs. electrostatic stabilization of nanoparticles.

Commonly used polymers in stabilizing metal nanoparticles include but are not limited to polyethylene glycol (PEG), polyvinylpyrrolidone (PVP) and polyvinyl alcohol (PVA). These three polymers have been analyzed previously for the nanoparticle sizes and reaction rate constants (Table 13). PEG was the stabilizing agent that gave the highest *k*, while PVA allowed the formation of nanoparticles in the smallest dimensions of 2-3 nm. Within the same polymer stabilizer, especially for PVA and PVP, the smaller the nanoparticle size the higher the *k*. Because the nature of the polymer affects the dimensions and activity of the catalyst, one type of polymer stabilizer

was selected to use for each test. PEG was used for the series of reusability tests due to it giving the higher *k*, whereas PVA was used for all other tests.

Table 13. *k* values and nanoparticle sizes of Au/AC catalysts with different stabilizers.

Sample	k (min^{-1})	Nanoparticle size (nm)
Au/AC PEG 0.3	0.048	10.3
Au/AC PEG 0.65	0.087	6.4
Au/AC PEG 1.2	0.088	6.2
Au/AC PEG 2.4	0.061	8
Au/AC PVP 0.3	0.078	6.7
Au/AC PVP 0.65	0.049	6.4
Au/AC PVP 1.2	0.028	8.2
Au/AC PVP 2.4	0.011	8.1
Au/AC PVA 0.3	0.036	3.6
Au/AC PVA 0.65	0.037	3.1
Au/AC PVA 1.2	0.039	2.6
Au/AC PVA 2.4	0.059	2.2
Au/AC PVA 0	0.047	6.4

3.10 Catalyst Reusability

A recovery and reusability method of the catalyst using PEG as a stabilizing agent was tested using the non-stirring cuvette setup to determine its suitability. Conversions for the initial and 5 reuse reactions are compared in Figure 28. Although the initial reaction and first reuse yielded similar conversion rates with near complete conversion within 20 min, significant decreases in conversion rates are seen in subsequent reuses with the last reaction yielding only 25% conversion in 1 h. It is noted that small particles of catalyst were observed suspended in liquid phase after centrifugation. The drastic loss of activity by the 3rd reuse may, therefore, mainly be due to the loss of catalyst during recovery than from the deactivation of the catalyst. However, it may be assumed that the active sites at the surface of the catalyst over several reuses become saturated. To avoid the poisoning of active sites, a washing step must be added after each cycle. Another possible

assumption is the agglomeration of the nanoparticles that would decrease the activity. A TEM analysis of the recovered catalyst for any change in particle size distribution would confirm or eliminate this hypothesis.

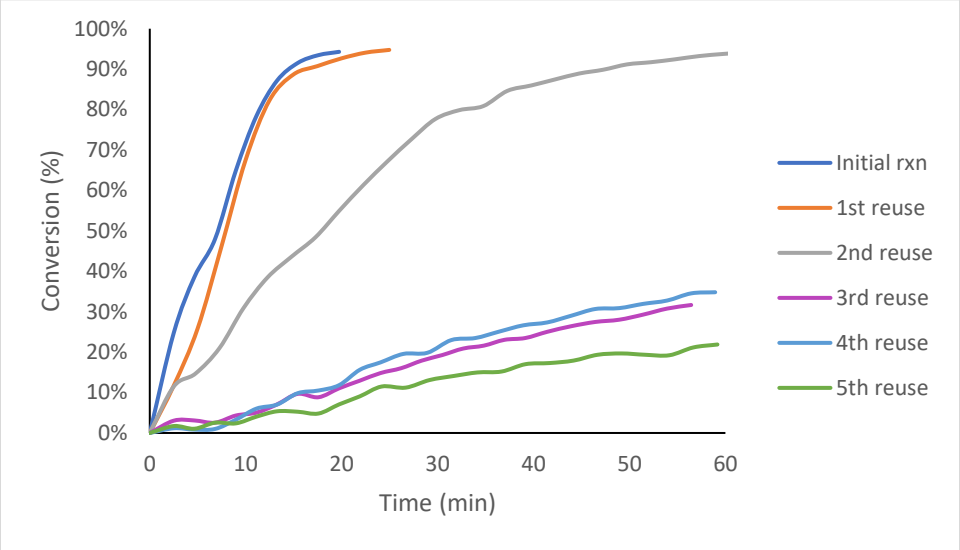

Figure 28. Reusability test with decrease in 4-nitrophenol conversion over 5 reuses.

3.11 Effect of support-substrate adsorption

It has been shown from previous studies from our team that AC, with its high surface area, adsorbs some of the 4-nitrophenol during the reaction. 4-nitrophenol reduction was analyzed with AC in place of the catalyst to show that the total adsorption of 4-nitrophenol onto AC was 90% using 16 mg of AC and stirring during reaction, 40% using 4 mg of AC and stirring during reaction, and 25% using 4 mg of AC and eliminating stirring during reaction. Therefore, to minimize this effect of the support, the amount of catalyst added to the reaction was decreased from 16 mg to 4 mg, and the reaction was performed without stirring. The adsorption of 4-nitrophenol by activated carbon compared to the conversion of 4-nitrophenol by the catalyst during a typical reaction is shown in Figure 29.

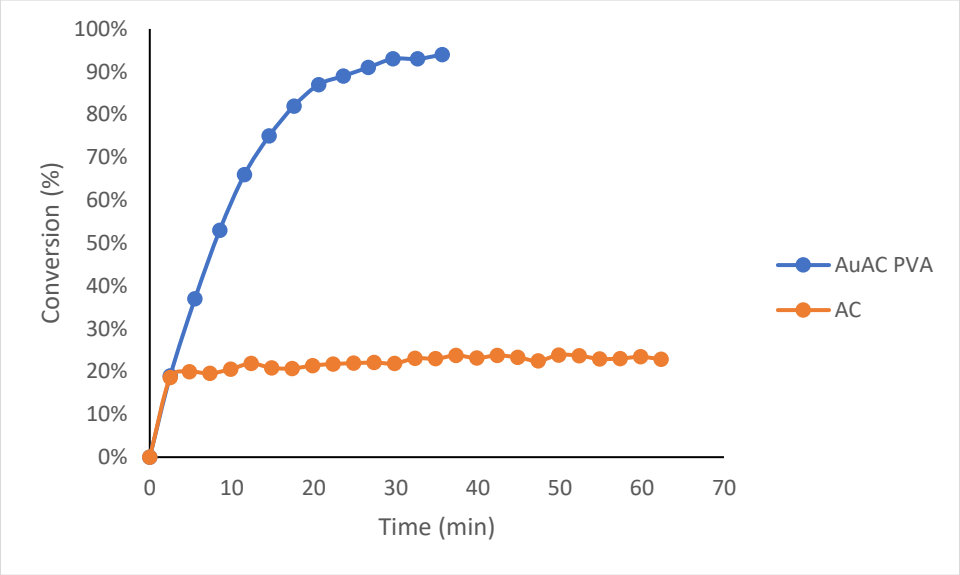

Figure 29. Adsorption of 4-nitrophenol by AC compared to that by Au/AC + PVA.

3.12 Biochar support as replacement for AC

Carbon materials have been widely used as a catalyst or as a catalyst support. Their large surface area, highly porous structure, electronic conductivity and chemical inertness allows it to be effective at reducing metals while being stable under acidic or basic environments or at high temperatures. They are a more affordable option compared to other common supports such as alumina and silica, while providing the versatility in shape and pore sizes which can be controlled during synthesis.[53] Activated carbon is one of the most used carbon materials as a metal nanoparticle support.

Taking the remediation of wastewaters through 4-nitrophenol reduction an extra step towards green chemistry, biochar obtained from the pyrolysis of various types of biomass is a newly researched topic. Biochar, charcoal derived from waste biomass, is obtained by pyrolysis in an oxygen-limited environment from renewable feedstock. Biochar provides many advantages over

the conventional activated carbon from coal coke. The utilization of biochar in catalysis presents a sustainable, more integrated process in biomass refining as emissions of CO_2, H_2S, SO_2 and NO_x are less.[54]

Biochar can be produced from wood, grass, manure, agricultural waste, municipal solid waste, or bones. The nature of the biochar strongly depends on the processing conditions such as the mineral and organic content of the feedstock and the pyrolysis temperature. Pyrolysis temperature influences the pore size and surface area of the biochar. The higher the pyrolysis temperature, the volatiles are released from the surface of the biomass, creating more pores and a larger surface area.[54] At temperatures above 500℃, the biochar contains the highest amount of condensed aromatic carbon which exhibits high stability over time.[8] The use of carbonaceous materials from agricultural waste for applications in industry is of much interest due to the widespread availability, low cost and environmental implications. In this specific study, the significance of biochar as carbon support lies in its low surface area compared to activated carbon. While AC is processed to have small pore sizes for a high surface area for efficient adsorption, experimental data showed high adsorption of the 4-nitrophenol during reaction. Using biochar samples with a much lower surface area provides one way of preventing 4-nitrophenol adsorption by the support, thus enabling solely the visualization of the catalyst activity in 4-nitrophenol reduction.

Besides its function as a support for dispersal and stabilization of metals, biochar may also work as a reducing agent to convert metal oxides to the metallic state.[54] Also, the presence of inorganic species may play a positive or negative role in biochar as a catalyst support. Inorganic content of biochar depends predominantly on the composition of the raw biomass. The presence of some inorganic elements may catalyze the pyrolysis process, increasing the biochar yield. On the other

hand, it has also been reported that high inorganic content in the biomass led to slower formation of stable polycyclic aromatic carbons, resulting in low stability of biochar.[55]

In a study conducted on the adsorption of 4-nitrophenol onto biochar from recycled pine sawdust, a higher pyrolysis temperature of the char resulted in a larger surface area, higher aromaticity and lower hydrophobicity, making the char more effective in the adsorption of 4-nitrophenol.[56]

In another study with regards to nanoparticle support, Pd nanoparticles with Fe-biochar from the pyrolysis of sawdust with preloaded Fe were tested in the reduction of 4-nitrophenol with $NaBH_4$.[57] During the reaction, the activity of Pd on Fe-biochar was superior than that of Pd on activated carbon at a certain Pd loading. The reusability of the Pd on Fe-biochar catalyst was successful via magnetic separation, with 90% of initial activity after 5 reuses.

Previous studies have shown that AC adsorbs a significant amount of 4-NP during the reaction. Biochar as a replacement for AC was tested to see whether it also adsorbs 4-NP. Three different catalysts were also synthesized using biochar: no PVA, 0.05 and 0.1 weight ratio of PVA to Au.

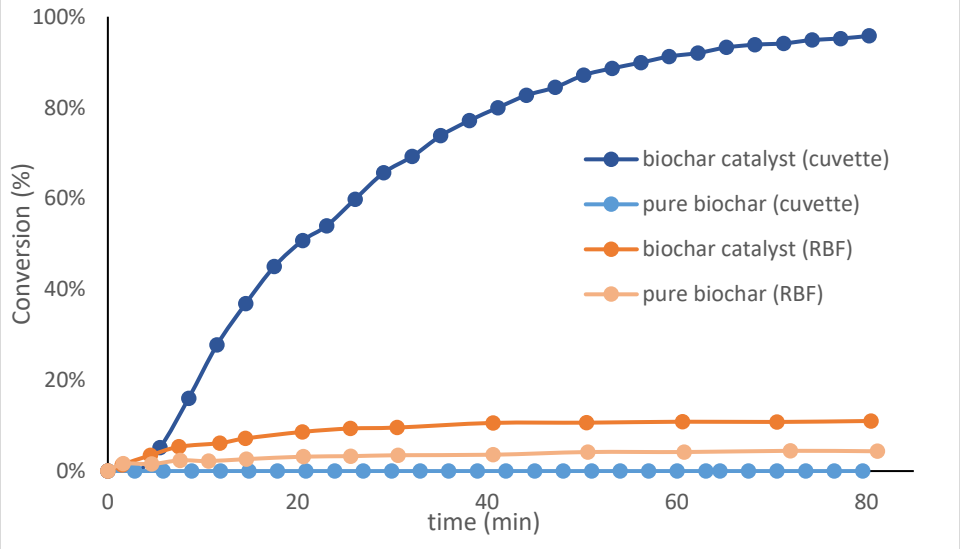

Figure 30. Comparison of conversion using biochar catalysts using the non-stirring (cuvette) vs. stirring (round-bottom flask) setup.

Figure 30 shows that in both reaction setups with and without stirring, the adsorption with biochar was lower, with approximately 0-4%. In comparing the two reaction setups, the non-stirring setup with the biochar catalyst yielded a significantly higher conversion rate, with no adsorption of 4-nitrophenol by the pure biochar. As observed in the AC catalyst, the higher conversion using the non-stirring setup was unexpected. Figure 30 shows that for pure carbon the stirring setup yields higher conversion, while the catalyst exhibits the opposite behavior. Therefore, the possibility of deactivation or leaching of the gold nanoparticles during the reaction was considered. A modification of this setup should also be investigated for the biochar to confirm whether the result is due to the performance of the nanoparticles or a flaw in the reaction setup.

Figure 31 reports the comparison among Au/AC and Au/Bioc catalysts with different amounts of PVA. The Au/AC catalyst exhibited the highest conversion rate, although the adsorption by AC itself should be considered. Pure AC adsorbs approximately 20-25% of the 4-nitrophenol, whereas pure biochar adsorbs anywhere from 0-4%. This result shows promise in the potential for biochar as catalyst support in place of AC. The subtraction of the adsorption effect of carbon is not necessary for an accurate analysis of the performance of the nanoparticles. Au/Bioc PVA 0 and Au/Bioc PVA 0.1 exhibited similar activity, whereas the Au/Bioc PVA 0.05 exhibited poor activity. Following these results, a reproducibility test was performed for each biochar catalyst to check for inconsistent activity (Figure 32).

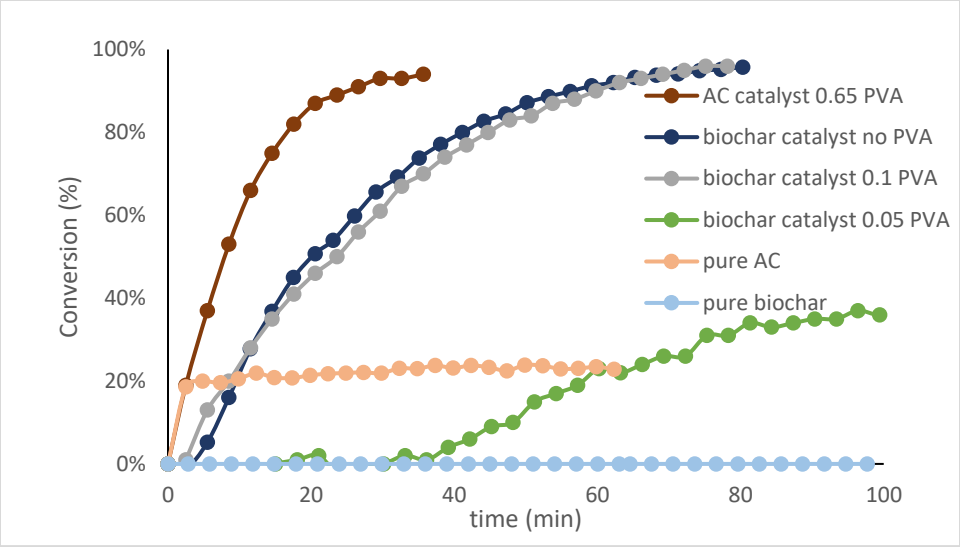

Figure 31. Conversion with AC catalyst vs. biochar catalysts with different amounts of PVA using the non-stirring reaction setup.

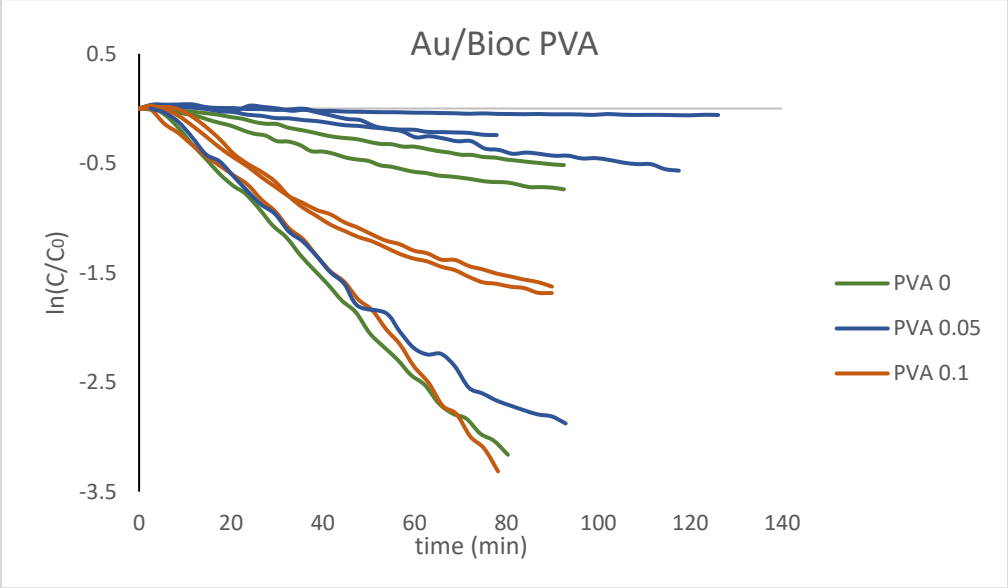

Figure 32. Comparison of reaction rates between biochar catalysts with differing amounts of PVA.

Table 14. Comparison of average *k* values with standard deviation between biochar catalysts with differing amounts of PVA.

Biochar catalyst	**Average *k* (min^{-1}) ±SD**
Au/Bioc PVA 0	0.0190 ±0.0164
Au/Bioc PVA 0.05	0.0112 ±0.0135
Au/Bioc PVA 0.1	0.0278 ±0.0106

From Figure 32 and Table 14, it is shown that the catalysts Au/Bioc PVA 0 and Au/Bioc PVA 0.05 display low *k* values with high standard deviations. The inconsistency in activity in these two catalysts could be attributed to insufficient amounts of PVA to produce uniform nanoparticles. With such a small quantity of catalyst used in the reaction and small amounts of PVA, the catalyst is not homogeneously dispersed. Therefore, the particle size distribution would be wider, resulting in drastically different activity each trial. The high *k* and low standard deviation of the Au/Bioc PVA 0.1 shows that the high amount of stabilizer results in a more active catalyst with high reproducibility from one test to another.

To properly compare the activities of Au/AC and Au/Bioc, Au/Bioc PVA 0.65 was prepared so that the amount of PVA is the same. However, preparation of a biochar catalyst with a PVA:Au weight ratio 0.65 was unsuccessful as seen from the residual pink/purple color of the solution following filtration (Figure 33). It was hypothesized that the interaction between -OH groups on PVA and the carbon hindered the immobilization of the AuNPs onto the biochar. However, the concern with eliminating the PVA stabilizer is the potential agglomeration and growth of the AuNPs, resulting in poor catalyst activity. A wide range of NP size distribution could also yield, to a certain degree, inconsistent activity from one test to another.

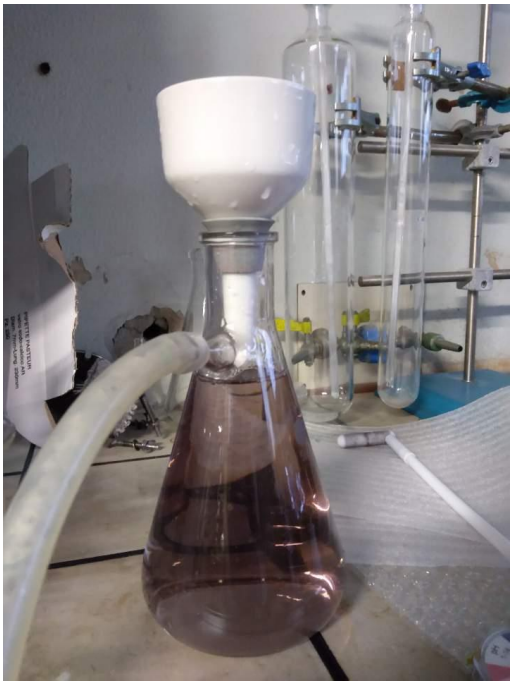

Figure 33. Filtered solution with high amounts of PVA leading to residual color.

Table 15 compares the average *k* values of Au/AC and Au/Bioc catalysts with different amounts of PVA for a comprehensive overview. The Au/AC catalysts show superior performance with and without PVA. However, it is noted that reproducibility tests were not performed with the Au/AC catalysts.

Table 15. Comparison of average *k* values with standard deviation among biochar catalysts and AC catalysts with differing amounts of PVA.

Catalyst	**Average *k* (min^{-1}) ±SD**
Au/AC PVA 0	0.0470 ± NA
Au/AC PVA 0.65	0.0794 ± NA
Au/Bioc PVA 0	0.0190 ±0.0164
Au/Bioc PVA 0.05	0.0112 ±0.0135
Au/Bioc PVA 0.1	0.0278 ±0.0106

4. Conclusions and suggestions for future work

Metal nanoparticles offer an extraordinarily wide range of factors to explore, including combinations of metals, supports and stabilizers, modes of preparations, and more. Among the investigated metals, gold nanoparticles are chosen for their high stability and reactivity in ambient conditions, showing promise in an increasing role in catalysis. The experimental and literature review sections of this paper highlighted the effects of supports and stabilizers on metal nanoparticle catalysts, as well as synergistic effects of metals. Activated carbon / biochar supported gold nanoparticles were prepared using the sol immobilization technique. Average particle sizes of Au/AC PVA0.65, Au/AC PVA0 and Au/biochar PVA0 analyzed with TEM were 2.4±1.6 nm, 8.9 ±11.5 and 5.8±2.3 nm, respectively. Among the Au/biochar catalysts, although it was seen that the absence of PVA led to higher nanoparticle sizes, there was little difference in the activities. Au/biochar PVA0.1 showed the highest activity, with a *k* value of 0.0278 compared to 0.0794 of Au/AC PVA0.65. A consideration when comparing these values is that biochar did not adsorb any 4-nitrophenol, whereas AC adsorbed 20-25% of the 4-nitrophenol. For biochar-supported metal nanoparticle catalysts to be applied industrially, a better understanding of the properties of biochar as support and its correlation with catalytic activity must be achieved. Due to the differences in behavior of biochar and activated carbon, modifications of the standard procedure of catalyst synthesis to yield well-dispersed, small nanoparticles is critical.

Reaction conditions and setups of 4-nitrophenol reduction were also tested. Regarding the stabilities of test solutions, the necessity to prepare fresh solutions with fresh chemicals was established. The stability of the catalyst was also tested, showing a noticeable difference in activity over a 1-year period. Comparing the reaction with and without stirring, the unexpected result of

higher conversion with the non-stirring method may point to a sampling flaw or the possibility of deactivation or leaching of gold nanoparticles during the reaction.

Some suggestions for continuation of this research include preparing the Au/AC catalyst with the same amount of PVA as the Au/biochar sample. Comparing Au/AC PVA 0.1 (PVA:Au weight ratio) with Au/biochar PVA 0.1 will allow to properly compare the functions of the support and determine the suitability of biochar as a replacement for AC.

A catalyst reusability test which involves a washing step after each cycle while minimizing the transfer of sample solution to avoid loss of catalyst would allow to check for catalyst deactivation. Furthermore, ICP-AES analysis of the catalyst by quantifying metal loading in the solution post-reaction would provide evidence of gold nanoparticle leaching, resulting in loss of catalyst activity.

5. Bibliography

1. Rampino, L. D. and Nord, F. F. Preparation of palladium and platinum synthetic high polymer catalysts and the relationship between particle size and rate of hydrogenation. *J. Am. Chem. Soc.* **63** (10), 2745-2749 (1941).
2. Haruta, M. *et al*. Novel gold catalysts for the oxidation of carbon monoxide at a temperature far below 0° C. *Chemistry Letters*, 405-408 (1987).
3. Astruc, D. Introduction: nanoparticles in catalysis. *Chem. Rev.* **120** (2), 461-463 (2020).
4. Saha, S. *et al.* Photochemical green synthesis of calcium-alginate-stabilized Ag and Au nanoparticles and their catalytic application to 4-nitrophenol reduction. *Langmuir* **26** (4), 2885-2893 (2010).
5. Shen, W. *et al*. Catalytic reduction of 4-nitrophenol using gold nanoparticles biosynthesized by cell-free extracts of *Aspergillus sp.* WL-Au. *Journal of Hazardous Materials* **321**, 299-306 (2017).
6. Rodrigues, C. S. D. *et al*. Wastewater treatment by catalytic wet peroxidation using nano gold-based catalysts: A review. *Catalysts* **9**, 478 (2019).
7. Ansar, S. M. and Kitchens, C. L. Impact of gold nanoparticle stabilizing ligands on the colloidal catalytic reduction of 4-nitrophenol. *ACS Catal*. **6**, 5553-5560 (2016).
8. Joseph, S. *et al.* Biochar production from agricultural and forestry wastes and microbial interactions. *Current Developments in Biotechnology and Bioengineering: Solid Waste Management* 443-473 (2017).
9. Sun, J. *et al*. Catalytic hydrogenation of nitrophenols and nitrotoluenes over a palladium/graphene nanocomposite. *Catal. Sci. Technol*. **4**, 1742 (2014).
10. Zhong, C. J. and Regalbuto, J. R. Metal nanoparticle synthesis. *Comprehensive Inorganic Chemistry II* **7**, 75-102 (2013).
11. Alshammari, A. S. Heterogeneous gold catalysis: from discovery to applications. *Catalysts* **9**(5), 402 (2019).
12. Ivanova, S. *et al*. A new preparation method for the formation of gold nanoparticles on an oxide support. *Applied Catalysis A: General* **267**, 191-201 (2014).
13. Berg, J. M *et al*. The relationship between pH and zeta potential of ~ 30 nm metal oxide nanoparticle suspensions relevant to *in vitro* toxicological evaluations. *Nanotoxicology* **3**(4), 276-283 (2009).
14. Zheng, N. and Stucky, G. D. A general synthetic strategy for oxide-supported metal nanoparticle catalysts. *J. Am. Chem. Soc.* **128**, 14278-14280 (2006).
15. Villa, A. *et al*. Sol immobilization technique: a delicate balance between activity, selectivity and stability of gold catalysts. *Catalysis Science & Technology* **3** (11), 3036 (2013).
16. Sun, Z. *et al*. Multifunctional dendritic mesoporous silica nanospheres loaded with silver nanoparticles as a highly active and recyclable heterogeneous catalyst. *Colloids and Surfaces A: Physicochem. Eng. Aspects* **489**, 142-153 (2016).
17. Oturan, M. A. *et al*. Complete destruction of *p*-nitrophenol in aqueous medium by electro-Fenton method. *Environ. Sci. Technol.* **34**, 3474-3479 (2000).
18. Aditya, T. *et al*. Remarkable facet selective reduction of 4-nitrophenol by morphologically tailored (111) faceted Cu_2O nanocatalyst. *ACS Omega* **2**, 1968-1984 (2017).
19. Bingwa, N. *et al*. Synergistic effects of gold-palladium nanoalloys and reducible supports on the catalytic reduction of 4-nitrophenol. *Langmuir* **33**, 7086-7095 (2017).
20. Kulkarni, M. and Chaudhari, A. Microbial remediation of nitro-aromatic compounds: an overview. *Journal of Environmental Management* **85**, 496-512 (2007).
21. Cuerda-Correa, E. M. *et al*. Advanced oxidation processes for the removal of antibiotics from water. An overview. *Water* **12**, 102 (2020).
22. Kavitha, V. and Palanivelu, K. Degradation of nitrophenols by Fenton and photo-Fenton processes. *Journal of Photochemistry and Photobiology A: Chemistry* **170**, 83-95 (2005).
23. Fatima, R. *et al*. Photocatalytic degradation performance of various types of modified TiO_2 against nitrophenols in aqueous systems. *Journal of Cleaner Production* **231**, 899-912 (2019).

24. Yu, C. P. and Yu, Y. H. Mechanisms of the reaction of ozone with *p*-nitrophenol. *Ozone: Science & Engineering: The Journal of the International Ozone Association* **23** (4), 303-312 (2007).
25. Farzadkia, M. *et al*. Catalytic ozonation of phenolic wastewater: identification and toxicity of intermediates. *Journal of Engineering* **2014**, Article ID 520929 (2014).
26. Jung, H. *et al*. Preparation of biotic and abiotic iron oxide nanoparticles (IOnPs) and their properties and applications in heterogeneous catalytic oxidation. *Environ. Sci. Technol.* **41**, 4741-4747 (2007).
27. Wu, Z. *et al*. Enhanced effect of suction-cavitation on the ozonation of phenol. *Journal of Hazardous Materials* **190**, 375-380 (2011).
28. Shanthi, S. Catalytic ozonation: an advanced strategy for the removal of nitro phenols from contaminated water. *J. Adv. Chem. Eng.* **7**, 168 (2017).
29. Yeber, M. C. *et al*. Photocatalytic degradation of cellulose bleaching effluent by supported TiO_2 and ZnO. *Chemosphere* **41**, 1193-1197 (2009).
30. Kazakov, D. A. *et al*. Catalytic ozonation of 4-nitrophenol in the presence of magnetically separable titanium dioxide – magnetite composite. *Eurasian Chemico-Technological Journal* **17**, 309-316 (2015).
31. Tabatabaei, S. M. *et al*. Enhancement of 4-nitrophenol ozonation in water by nano ZnO catalyst. *Iran. J. Environ. Health. Sci. Eng.* **8** (4), (2011).
32. Jung, H. and Choi, H. Catalytic decomposition of ozone and *para*-chlorobenzoic acid (*p*CBA) in the presence of nanosized ZnO. *Applied Catalysis B: Environmental* **66**, 288-294 (2006).
33. Shokri, A. Degradation of 4-nitrophenol from industrial wastewater by nano catalytic ozonation. *Int. J. Nano Dimens.* **7** (2), 160-167 (2016).
34. Corbett, J. F. An historical review of the use of dye precursors in the formulation of commercial oxidation hair dyes. *Dyes and Pigments* **41**, 127-136 (1999).
35. Wunder, S. *et al*. Kinetic analysis of catalytic reduction of 4-nitrophenol by metallic nanoparticles immobilized in spherical polyelectrolyte brushes. *J. Phys. Chem. C* **114**, 8814-8820 (2010).
36. Zhao, P. *et al.* Basic concepts and recent advances in nitrophenol reduction by gold- and other transition metal nanoparticles. *Coordination Chemistry Reviews* **287**, 114-136 (2015).
37. Cheong, S. *et al*. Shape control of platinum and palladium nanoparticles for catalysis. *Nanoscale* **2** (10), 2045 (2010).
38. Bell, A. T. The impact of nanoscience on heterogeneous catalysis. *Science* **299**, 1688 (2003).
39. Li, W. *et al*. Silica-supported Au-Cu alloy nanoparticles as an efficient catalyst for selective oxidation of alcohols. *Applied Catalysis A: General* **433-434**, 146-151 (2012).
40. Hummers Jr, W. S. and Offeman, R. E. Preparation of graphitic oxide. *Journal of the American Chemical Society* **80** (6), 1339 (1958).
41. Chen, X. *et al*. AuPd bimetallic nanoparticles decorated on graphene nanosheets: their green synthesis, growth mechanism and high catalytic ability in 4-nitrophenol reduction. *J. Mater. Chem. A.* **2**, 5668-5674 (2014).
42. Cote, L. J. *et al.* Langmuir-Blodgett assembly of graphite oxide single layers. *J. Am. Chem. Soc.* **131**, 1043-1049 (2009).
43. Saha, S. *et al.* Photochemical green synthesis of calcium-alginate-stabilized Ag and Au nanoparticles and their catalytic application to 4-nitrophenol reduction. *Langmuir* **26** (4), 2885-2893 (2010).
44. Maji, T. *et al*. *In situ* synthesis of ultra-small platinum nanoparticles using water soluble polyphenolic polymer with high catalytic activity. *RSC Adv.* **4** (93), 51745-51753 (2014).
45. Berahim, N. *et al*. Synthesis of bimetallic gold-silver (Au-Ag) nanoparticles for the catalytic reduction of 4-nitrophenol to 4-aminophenol. *Catalysts* **18**, 412 (2018).
46. Monga, A. and Pal, B. Improved catalytic activity and surface electro-kinetics of bimetallic Au-Ag core-shell nanocomposites. *New Journal of Chemistry* **39** (1), 304-313 (2015).
47. Mehmood, S. *et al*. AuCu@Pt nanoalloys for catalytic application in reduction of 4-nitrophenol. *Journal of Spectroscopy* **2016**, Article ID 621794 (2016).
48. Suwannarat, K. *et al*. Synthesis of hollow trimetallic Ag/Au/Pd nanoparticles for reduction of 4-nitrophenol. *Colloids and Surfaces A: Physicochemical and Engineering Aspects* **540**, 73-80 (2018).
49. Wan, Y. *et al*. Quasi-spherical silver nanoparticles: aqueous synthesis and size control by the seed-mediated Lee-Meisel method. *Journal of Colloid and Interface Science* **394**, 263-268 (2013).

50. Thongthai, K. *et al*. Ag/Au/Pt trimetallic nanoparticles with defects: preparation, characterization, and electrocatalytic activity in methanol oxidation. *Nanotechnology* **28** (37), 375602 (2017).
51. Frens, G. Controlled nucleation for the regulation of the particle size in monodisperse gold suspensions. *Nature Physical Science* **241**, 20-22 (1973).
52. Srisombat, L. *et al*. Simple preparation Au/Pd core/shell nanoparticles for 4-nitrophenol reduction. *Colloids and Surfaces A: Physicochem. Eng. Aspects* **512**, 17-25 (2017).
53. Gerber, I. C. and Serp, P. A theory/experience description of support effects in carbon-supported catalysts. *Chem. Rev.* **120** (2), 1250-1349 (2020).
54. Cheng, F. and Li, X. Preparation and application of biochar-based catalysts for biofuel production. *Catalysts* **8**, 346 (2018).
55. McBeath, A. V. *et al*. Influence of feedstock properties and pyrolysis conditions on biochar carbon stability as determined by hydrogen pyrolysis. *Biomass and Bioenergy* **73**, 155-173 (2015).
56. Liu, L. *et al*. Adsorption characteristics and mechanism of p-nitrophenol by pine sawdust biochar samples produced at different pyrolysis temperatures. *Scientific Reports* **10**, 5149 (2020).
57. Jiang, S. F. *et al*. Biochar-supported magnetic noble metallic nanoparticles for the fast recovery of excessive reductant during pollutant reduction. *Chemosphere* **227**, 63-71 (2019).
58. Munnik, P. *et al*. Recent developments in the synthesis of supported catalysts. *Chem. Rev.* **115**, 6687-6718 (2015).
59. Dieckmann, M. S. and Gray, K. A. A comparison of the degradation of 4-nitrophenol via direct and sensitized photocatalysis in TiO_2 slurries. *Water Research* **30** (5), 1169-1183 (1996).
60. Zhang, J. *et al*. Highly active PtAu alloy nanoparticle catalysts for the reduction of 4-nitrophenol. *Nanoscale* **6**, 2125-2130 (2014).
61. Johnson, J. A. *et al*. Size-dependent hydrogenation of *p*-nitrophenol with Pd nanoparticles synthesized with poly(amido)amine dendrimer templates. *The Journal of Physical Chemistry C* **117** (44), 22644-22651 (2013).
62. Cui, Y. *et al*. Polyethyleneimine-stabilized palladium nanoparticles for reduction of 4-nitrophenol. *Transition Metal Chemistry* **44**, 655-662 (2019).
63. Wang, B. *et al*. Application of heterogeneous catalytic ozonation for refractory organics in wastewater. *Catalysts* **9**, 241 (2019).
64. Nawaz, F. *et al*. Catalytic ozonation of 4-nitrophenol over an mesoporous α-MnO_2 with resistance to leaching. *Catalysis Today* **258**, 595-601 (2015).
65. Nawaz, F. *et al*. Selection of active phase of MnO_2 for catalytic ozonation of 4-nitrophenol. *Chemosphere* **168**, 1457-1466 (2017).
66. Feng, X. H. *et al*. Synthesis of todorokite at atmospheric pressure. *Chem. Mater.* **16**, 4330-4336 (2004).
67. Bajpai, S. K. *et al*. Synthesis of polymer stabilized silver and gold nanostructures. *J. Nanosci. Nanotechnol.* **7**, 2994-3010 (2007).
68. Cho, E. C. *et al*. Understanding the role of surface charges in cellular adsorption versus internalization by selectively removing gold nanoparticles on the cell surface with a I_2/KI etchant. *Nano Lett.* **9**, 1080-1084 (2009).
69. Torres, E. *et al*. Gold and silver uptake and nanoprecipitation on calcium alginate beads. *Langmuir* **21** (17), 7951-7958 (2005).
70. Daniel, M. C. and Astruc, D. Gold nanoparticles: assembly, supramolecular chemistry, quantum-size-related properties, and applications toward biology, catalysis, and nanotechnology. *Chem. Rev.* **104**, 293-346 (2004).
71. Lee, J. *et al*. Biochar as a catalyst. *Renewable and Sustainable Energy Reviews* **77**, 70-79 (2017).
72. Gu, L. *et al*. Degradation of aqueous *p*-nitrophenol by ozonation integrated with activated carbon. *Ind. Eng. Chem. Res.* **47**, 6809-6815 (2008).
73. Wang, A. *et al*. Understanding the synergistic effects of gold bimetallic catalysts. *Journal of Catalysis* **308**, 258-271 (2013).